White Rose Research Online

eprints@whiterose.ac.uk
https://eprints.whiterose.ac.uk
Universities of Leeds, Sheffield and York

Deposited via The University of Sheffield.

White Rose Research Online URL for this paper:
https://eprints.whiterose.ac.uk/id/eprint/237469/

Version: Published Version

Article:
Eskandarinia, M., Adesanya, E., Walkley, B. et al. (2026) New insight into the reactivity of steel slags: Effect of post-milling duration. Journal of Sustainable Metallurgy. ISSN: 2199-3823

https://doi.org/10.1007/s40831-026-01421-2

Reuse
This article is distributed under the terms of the Creative Commons Attribution (CC BY) licence. This licence allows you to distribute, remix, tweak, and build upon the work, even commercially, as long as you credit the authors for the original work. More information and the full terms of the licence here:
https://creativecommons.org/licenses/

Takedown
If you consider content in White Rose Research Online to be in breach of UK law, please notify us by emailing eprints@whiterose.ac.uk including the URL of the record and the reason for the withdrawal request.

UNIVERSITY OF LEEDS
University of Sheffield
UNIVERSITY of York

Journal of Sustainable Metallurgy
https://doi.org/10.1007/s40831-026-01421-2

THEMATIC SECTION: 9TH INTERNATIONAL SLAG VALORISATION SYMPOSIUM

New Insight into the Reactivity of Steel Slags: Effect of Post-milling Duration

Milad Eskandarinia[1] · Elijah Adesanya[1] · Brant Walkley[2] · Juho Yliniemi[1]

Received: 25 September 2025 / Accepted: 9 January 2026
© The Author(s) 2026

Abstract

Incorporating steel slag, a residue derived from the metallurgical industry, into cementitious systems offers a sustainable route for resource recovery and carbon footprint reduction. Milling has been reported to address the low cementitious reactivity of steel slag, which remains a significant barrier to its widespread adoption. However, the influence of storage duration after milling on steel slag performance has not been systematically evaluated. To investigate the effects of post-milling duration as an independent factor, two types of steel slag, derived from a basic oxygen furnace and an electric arc furnace processes, were milled using planetary ball milling and stored under controlled environmental conditions for 1 h, 1 day, 4 days, 7 days, 3 months, and 1 year. The results showed that prolonged storage caused significant particle agglomeration, detected by particle size analysis, and a slight reduction in reactivity after 1 year, as determined by the Rapid, Reliable Relevant (R^3) reactivity test for supplementary cementitious materials. Replacing 30% of cement with steel slags stored for different times (1 h vs. 1 year) changed the properties of the blends. Compared with freshly milled slag, slag stored for 1 year caused a slight delay in cement hydration, as evidenced by calorimetry results. Consequently, blends containing 1-year-stored slag exhibited prolonged setting times and reduced apparent viscosity compared with the 1-h slag–cement blends. The compressive strength of blended cements was also negatively affected by long-term storage, and the amount of hydration products, such as portlandite, was slightly reduced in 28-day composites containing 1-year-stored slag.

The contributing editor for this article was M. Akbar Rhamdhani.

✉ Juho Yliniemi
Juho.Yliniemi@oulu.fi

[1] Fibre and Particle Engineering Research Unit, University of Oulu, 90014 Oulu, Finland

[2] School of Chemical, Materials, and Biological Engineering, University of Sheffield, Sheffield S1 3JD, UK

Published online: 20 January 2026

Graphical Abstract

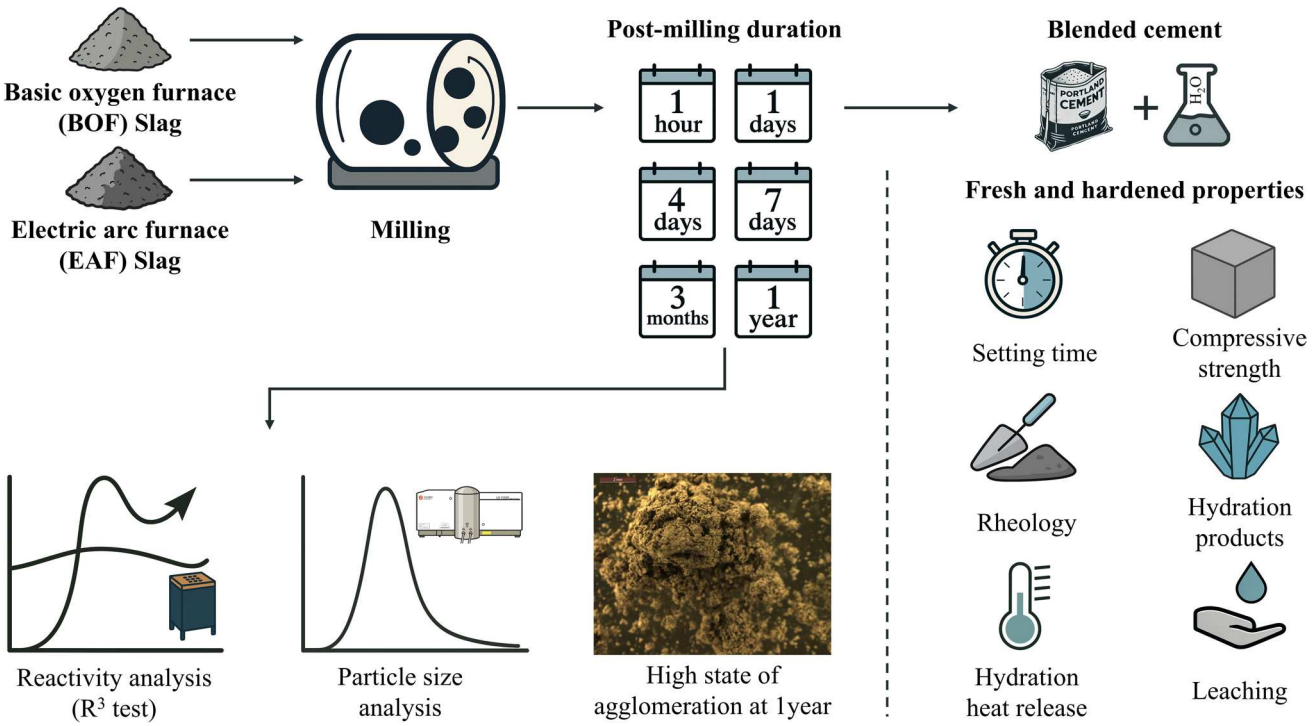

Keywords Steel slag · Milling · Post-milling duration · Supplementary cementitious material

Introduction

The steelmaking industry, operating predominantly via basic oxygen furnace (BOF) and electric arc furnace (EAF) processes, annually generates approximately 190–290 million tonnes of steel slags as of 2024 [1], corresponding about 15–20% of global crude steel output [2, 3]. The chemical composition of BOF slag is highly variable and depends on several factors, including the type of iron ore, flux additives, steelmaking process, and cooling conditions. In general, BOF slag contains approximately 40–60 wt% CaO, 10–20 wt% SiO_2, 20–30 wt% Fe_2O_3 (FeO/Fe), 1–6 wt% Al_2O_3, and 2–10 wt% MgO, together with minor oxides such as MnO, P_2O_5, Na_2O, and SO_3 [4]. The mineralogical composition of BOF slag typically comprises 30–60 wt% dicalcium silicate (C_2S, often containing 1–3 mol.% P_2O_5 substitution), 0–30 wt% tricalcium silicate (C_3S), 0–10 wt% free CaO (with 2–10 mol.% MnO and 5–15 mol.% FeO substitutions), 10–40 wt% wüstite (FeO) enriched with 10–20 mol.% MnO, 10–30 mol.% CaO, and 5–20 mol.% MgO, and 5–20 wt% dicalcium ferrite (C_2F) [5]. In contrast, EAF slag is generated mainly from steel scrap smelting, with minor additions of pig iron or direct-reduced iron. Because its feedstock composition is less uniform than that of the BOF process, EAF slag shows a wider range of chemical variability. The dominant crystalline phases typically include merwinite ($3CaO{\cdot}MgO{\cdot}2SiO_2$), wüstite, gehlenite ($Ca_2Al_2SiO_7$), kirschsteinite ($CaFeSiO_4$), dicalcium silicate, tricalcium silicate, mayenite ($Ca_{12}Al_{14}O_{33}$), brownmillerite (C_4AF), chromite ($FeCr_2O_4$), and magnetite (Fe_3O_4) [4, 6, 7]. The presence of calcium silicate phases such as dicalcium silicate (belite) and tricalcium silicate (alite), along with calcium aluminate and ferrite phases, imparts intrinsic cementitious potential to both BOF and EAF slags, making them promising candidates for use as supplementary cementitious materials (SCMs) in building applications [4].

The strategic valorization of steel slag within cementitious systems not only facilitates the partial substitution of Portland cement, which remains a major contributor to global CO_2 emissions [8], but also enables the integration of the steel sector into circular industrial networks. Furthermore, repurposing steel slag can mitigate the environmental risks of landfilling of steel slag, such as the leaching of trace metals that can adversely affect soil quality and groundwater integrity [9]. Nonetheless, the widespread adoption of steel slag as an SCM is impeded by its inherently low hydraulic reactivity. This limitation is primarily associated with

the presence of inert mineral phases such as the RO-phase (FeO–MgO–MnO solid solution), the highly crystalline microstructure, and the predominance of latent hydraulic phases such as γ-dicalcium silicate formed during the slow cooling process of steel slag [6].

Milling, while routinely employed in cement production to control fineness and reactivity, is regarded as a vital, efficient, and scalable approach to enhance the inherently low reactivity of steel slag by reducing particle size, increasing specific surface area, and inducing structural disorder [10–16]. Wang et al. [17] investigated the cementitious properties of steel slag subjected to milling, demonstrating that when the fineness was increased to a specific surface area of 786 $m^2 \cdot kg^{-1}$ (square meters per kilogram), the material exhibited a marked improvement in reactivity during the early and intermediate stages of hydration. Li et al. [18] reported that milling of steel slag under dry milling conditions refined the particle size and induced amorphization of the main crystal structures, including silicates, hydroxides, sulfates, aluminates, and ferrites, which, in turn, enhanced the hydration reactivity of the slag and markedly improved compressive strength, particularly at high water-to-solid ratios. Sun et al. [19] examined the influence of two activation methods (dry and wet milling) on the reactivity of steel slag and reported that both methods substantially reduced particle size and enhanced the reactivity of C_3A and C_3S; the effect was more pronounced under wet milling, which resulted in shortened setting times and strength improvements across all ages, with the most pronounced strength gain observed at 60 days. While reducing the particle size of steel slag through milling enhances its reactivity, this improvement does not increase linearly with fineness. Two main factors explain this behavior. First, the grinding process is highly energy demanding because of the presence of hard-to-grind minerals (iron-rich phases such as wüstite), which significantly increase both power consumption and CO_2 emissions as finer particle sizes are targeted [20–22]. Second, intensive and prolonged milling promotes particle agglomeration due to microcrack formation and structural disorder, which raise surface energy and induce electrostatic attraction among particles [23]. These effects reduce grinding efficiency and lead to a plateau in reactivity improvement. Therefore, an optimal balance between fineness, reactivity, energy cost, and environmental impact is essential. According to the 3E (engineering, environmental, and economic) optimization model proposed by Li et al. [24], the steel slag powder with an average particle size of 22.4 μm (micrometers) exhibited the best overall performance, while minimizing CO_2 emissions and energy consumption.

In practical process chains, milled steel slag powders are usually stored before use. A comparable situation occurs in the cement industry, where Portland cement (PC) clinker is often stored prior to grinding, and the ground cement is also stored for varying periods before use. It is well established that the unintentional exposure of cement to controlled or uncontrolled environments with moisture or reactive species such as CO_2 can modify the physical and chemical characteristics of the particles prior to mixing with water [25–29]. These alterations lead to an undesirable reactivity loss, resulting in slower setting, reduced hardening rates, and lower strength development in cementitious materials [30, 31]. Lv et al. [32] investigated the behavior of calcium sulfoaluminate (CSA) cement powders when exposed to controlled ambient relative humidities (RH) of 57%, 75%, and 97% for up to 90 days following milling prior to use in concrete. They reported that storage at 57% RH had a negligible effect on both cumulative heat release and compressive strength, with values remaining comparable to those of freshly ground cement. In contrast, at elevated humidity levels of 75% and 97%, both cumulative heat release and strength declined progressively with storage duration, a deterioration attributed to the gradual consumption of ye'elimite and anhydrite that ultimately resulted in a substantial reduction in the hydraulic activity of CSA cement. Stoian et al. [33] correlated the changes in reactivity and the evolution of strength in cement pastes with the effects of storing Portland cement under moisture exposure conditions for periods of 1–3 months. The reported reduction in reactivity has been associated with the formation of hydrated and carbonated surface layers on cement particles during storage, which act as mass-transport barriers that hinder water penetration and consequently slow subsequent hydration reactions.

Cieri et al. [34] examined the influence of prolonged storage of cement powder under uncontrolled conditions on the early age stiffness evolution of Portland (CEM II/A) and pozzolanic (CEM IV/B) cement pastes, and found that storage led to a measurable reduction in both Young's modulus and the rate of hardening, with these reductions becoming more pronounced as the storage period was extended up to 360 days. Although these studies were conducted on cement powders, similar physical and chemical phenomena may also occur in milled steel slags during storage. Both materials are susceptible to surface modification through exposure to moisture and CO_2, and particle agglomeration may reduce the availability of reactive sites. However, the effects differ in extent and rate due to compositional differences. Portland cement contains more reactive phases, such as alite, which can readily react under elevated humidity, whereas steel slags contain smaller amounts of such reactive phases and are richer in metal oxides. Consequently, these transformations in steel slags are expected to progress differently in extent and kinetics compared to Portland cement.

Although the time period between milling and use represents a potentially critical variable influencing the performance of ground steel slags in cementitious systems, it has not, to date, been investigated. This study aims to clarify

how the post-milling duration, defined as the period of storage between milling and incorporation into a cement matrix, affects the properties of the ground powder and its behavior as an SCM. Two distinct steel slag types, namely basic oxygen furnace (BOF) slag and electric arc furnace (EAF) slag, were milled (identical process) using a planetary ball mill and subsequently stored in sealed polyethylene containers placed in a desiccator at ambient temperature for periods ranging from 1 h to 1 year. The effects of post-milling duration were quantified through particle size distribution analysis and reactivity assessment using the Rapid, Reliable, and Relevant (R^3) test [35], as developed and standardized for SCMs. The practical implications of the changes that occurred during the post-milling period were then evaluated by partially replacing CEM I 52.5 N cement (30% by mass) with steel slags stored for either 1 h or 1 year. The fresh and hardened properties of the blended cements, including setting time, rheological behavior, hydration kinetics, compressive strength, and phase assemblage, were assessed, together with leaching performance to evaluate environmental implications.

The ultimate aim of this study is to provide operational guidance for the scheduling and handling of ground steel slag for its effective use as an SCM. This can enable large-scale valorization of steel slag, creating a direct link between the metallurgy and cement industries, where the residues of steel production are transformed into valuable constituents for cementless binders in the construction sector.

Materials and Methods

Materials

Two distinct steel slags, namely BOF and EAF slag from steelmaking processes, were utilized in this study. To ensure uniform initial particle size characteristics across all experimental replicates, each steel slag type was homogenized and subsequently subdivided into aliquots with equivalent particle size distribution using a spinning riffler (PT 100, Retsch). The particle size distributions of the homogenized steel slags before milling are presented in Fig. 1. Measurements were performed using an Alpine Air Jet Sieve (e200LS, Hosokawa Alpine) operated in time-controlled mode with a batch size of 90 g (grams). Each sieve fraction was tested for 1–8 min (minute) under a vacuum pressure of 2800–3700 Pa (pascal), covering the size range 25–2000 µm.

The X-ray diffraction (XRD) diagrams of the as-received steel slags and PC, CEM I 52.5 N (newton)) are presented in Fig. 2. The chemical compositions of the BOF and EAF slags, along with that of PC, were determined by X-ray fluorescence (XRF) using the borate fusion (fused bead) method.

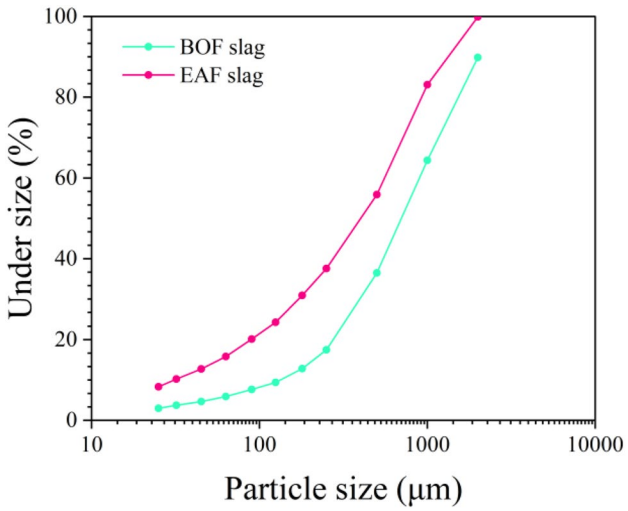

Fig. 1 Cumulative undersize curves of BOF and EAF slags prior to milling

Detailed results were reported in our earlier work [36], and the corresponding values are summarized in Table 1.

Material Preparation

Milling

The milling of BOF and EAF slags was performed using a planetary ball mill (PM 200, Retsch). In each test, 90 g of slag and 160 g of stainless steel milling media (25 balls, each 12.5 mm (millimeter) in diameter) were loaded into a 125 mL (milliliter) stainless steel milling bowl. Milling was conducted under dry conditions at a rotational speed of 450 min^{-1} (per minute) for 30 min. After milling, the slag powder was immediately transferred to airtight containers.

Post-milled Powder

To investigate the influence of post-milling duration on the characteristics of BOF and EAF slag powders, the milled samples were stored in sealed polyethylene containers placed in a desiccator at ambient temperature for varying durations: 1 h (1H), 1 day (1D), 4 days (4D), 7 days (7D), 3 months (3 M), and 1 year (1Y). The nomenclature of each powder sample was assigned according to both the type of slag and the post-milling storage period. For example, "1Y_EAF" denotes an EAF slag sample that had been milled and subsequently stored for one year prior to testing.

Paste

To evaluate the influence of post-milling duration on the performance of steel slag in cementitious composites, 30% of

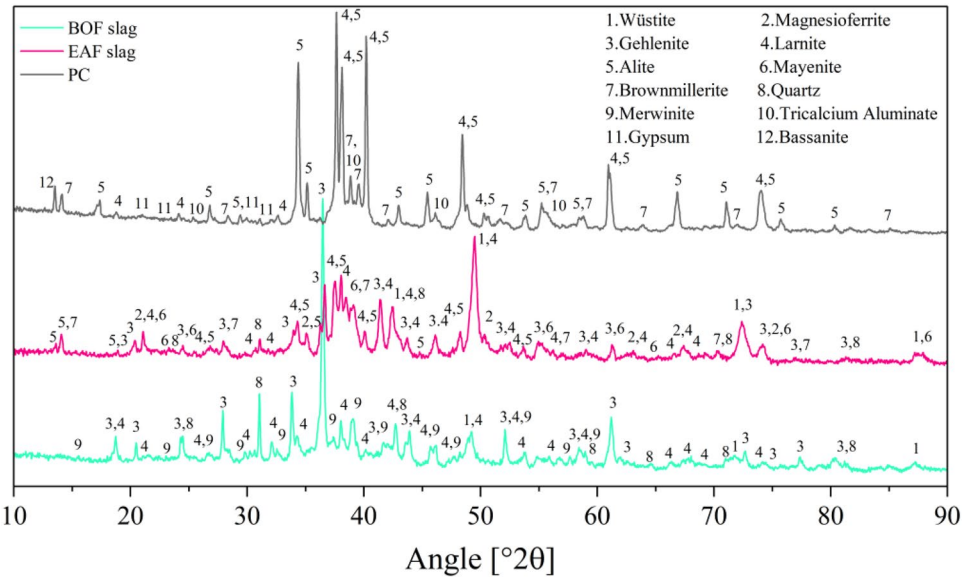

Fig. 2 Mineral composition of as-received steel slags and Portland cement

Table 1 Chemical composition (mass fraction, wt%)

Component	BOF slag	EAF slag	PC
Calcium oxide (CaO)	32.2	34.0	63.8
Aluminum oxide (Al_2O_3)	6.5	6.9	4.6
Silicon dioxide (SiO_2)	26.9	27.5	19.6
Magnesium oxide (MgO)	9.2	8.6	2.6
Iron oxide (Fe_2O_3)	16.2	13.6	3.9
Phosphorus pentoxide (P_2O_5)	0.3	0.4	0.1
Sulfur trioxide (SO_3)	1.2	0.9	3.6
Chromium oxide (Cr_2O_3)	0.6	1.0	0.0
Titanium dioxide (TiO_2)	0.4	0.4	0.2
Manganese oxide (MnO)	4.5	5.4	0.1
Minor oxides	0.8	1.0	1.7
Loss on ignition (LOI)	1.3	0.3	0.0

Table 2 Mix proportion of control cement and steel slag-blended mixtures

Sample ID	Portland cement	Steel slag			w/b
	wt%	Type	Post-milling duration	wt%	
CC_CRTL	100	–	–	–	0.45
CC_1H_BOF	70	BOF	1 Hour	30	0.45
CC_1Y_BOF	70	BOF	1 Year	30	0.45
CC_1H_EAF	70	EAF	1 Hour	30	0.45
CC_1Y_EAF	70	EAF	1 Year	30	0.45

w/b water to binder ratio

the Portland cement (by mass) was replaced with post-milled steel slag stored for 1 h and 1 year. The paste mix proportions are summarized in Table 2. All paste samples were prepared using a high-shear blender operating at 1600 min^{-1} for 2 min. After casting, the specimens were stored for 24 h at 20 °C (degree Celsius) and 60% relative humidity. Following demolding, the samples were cured in water until testing at the designated ages.

Analytical Methods

Characterization of Post-milled Steel Slag Powder

The particle size distributions of the milled steel slags at various post-milling durations were determined using a laser diffraction particle size analyzer (LS 13 320, Beckman Coulter). Prior to measurement, each powder sample was dispersed in pure isopropanol to prevent interaction of the particles with water during analysis, and each was subsequently subjected to ultrasonic treatment for 3 min.

The Rapid, Reliable, and Relevant (R^3) test was performed to examine the reactivity of milled steel slag powder as a function of post-milling duration, in accordance with ASTM C1897-20 [35]. For each measurement, milled steel slag corresponding to a specific post-milling duration was blended with calcium hydroxide ($Ca(OH)_2$), intended to promote pozzolanic activity, and calcium carbonate ($CaCO_3$), incorporated to facilitate reactions with aluminum species dissolved from the slag [37]. A solid blend containing 22.22 wt% milled steel slag, 66.66 wt% $Ca(OH)_2$, and 11.12 wt% $CaCO_3$ was homogenized using a mechanical mixer. The alkaline solution was prepared by dissolving potassium hydroxide (KOH) and potassium sulfate (K_2SO_4) in deionized water at room temperature, mimicking the pore

solution of slag–cement systems with dissolved ions such as SO_4^{2-} and OH^- [37]. The solution comprised 0.39 wt% KOH, 1.95 wt% K_2SO_4, and 97.66 wt% water. The solid mixes and alkaline solutions were preconditioned at 40 °C for 16 h prior to mixing to ensure thermal stabilization. Following preconditioning, the solids and solution were mixed at a liquid-to-solid mass ratio of 1.2, and 15 g of the resulting homogeneous paste was immediately transferred to airtight ampoules. The ampoules were placed in an isothermal calorimeter maintained at 40 °C to accelerate the reaction between slag and calcium hydroxide. After 7 days, the cumulative heat release per gram of SCM was calculated using Eq. (1).

$$H_{\text{steel slag}} = \frac{H}{m_p \times 0.101} \tag{1}$$

where H is cumulative heat release recorded by the isothermal calorimeter, m_p is the mass of the paste, and 0.101 is the mass fraction of SCM (steel slag) in the paste.

Paste samples were also cast in sealed 40 mL plastic bottles and cured in an oven at 40 °C for 7 days. At the specified curing age, the specimens were removed from the oven, and the top portion was cut off and discarded to minimize errors associated with paste segregation. The remaining paste was then placed back in the 40 °C oven for 24 h without sealing, as the material was too moist to pass through a 2 mm sieve. After drying, the specimens were ground (< 2 mm) and subsequently heated in a furnace at 350 °C for 2 h. The chemically bound water content (Method A) was calculated according to Eq. (2).

$$\text{Bound water (\%)} = \frac{w_0 - w_h}{w_0 - w_c} \times 100 \tag{2}$$

where w_0 is the total mass of the dried specimen and crucible, w_h is the total mass of the heated paste and crucible after cooling in a desiccator for 1 h, and w_c is the mass of the cooled empty crucible. Three replicate measurements were performed, and the average value was taken as the chemically bound water content.

Additionally, slices (approximately 3 g) cut from pastes cured at 40 °C for 7 days were immersed in 100 mL of pure isopropanol for 15 min. Excess isopropanol was removed by vacuum filtration, after which the samples were washed once with 20 mL of isopropanol and twice with 20 mL of diethyl ether. The washed samples were then dried in a ventilated oven at 40 °C for 8 min, in accordance with the RILEM TC-38 recommendation for hydration stoppage by solvent exchange [38]. The resulting powder, after additional grinding (< 63 µm), was subjected to thermogravimetric and derivative thermogravimetric (TG/DTG) analysis. Thermogravimetric measurements were performed using a NETZSCH STA 449 F3 TG/DSC instrument, in which the powder samples were heated from 40 °C to 1000 °C at a constant rate of 10 °C·min^{-1} (degree Celsius per minute) under a nitrogen atmosphere flowing at 10 mL·min^{-1}. The calcium hydroxide content was quantified from the mass loss between 400 °C and 500 °C using the tangential method described by Lothenbach et al. [39]. The calcium hydroxide consumption normalized per SCM (steel slag) mass was calculated from the difference between the initial portlandite content of the system and that remaining after 7 days [40]. The bound water content (Method B) was also calculated from thermogravimetric measurement based on Eq. (3):

$$\text{Bound water (\%)} = \frac{W_{40} - W_{550} - W_{H_2OCH}}{W_{550}} \tag{3}$$

where W_{40} is the sample mass at 40 °C, W_{550} is the sample weight at 550 °C, and $W_{H2O\text{-}CH}$ mass loss associated with the decomposition of portlandite (CH), calculated using the tangential method.

Characterization of Post-milled Steel Slag-Blended Cement

The rate of heat evolution and the cumulative heat release during 168 h of paste hydration were monitored using an isothermal calorimeter (TA Instruments). Fresh paste samples (7 g), prepared outside the calorimeter, were placed into airtight ampoules, while deionized water (3.04 g) in an identical ampoule served as the reference. Calorimetric measurements were conducted at a constant temperature of 23 °C. The initial and final setting times of the fresh pastes were determined in accordance with EN 196-3 [41], using an automated Vicat apparatus (Vicatronic, Matest E044N) at a controlled temperature of 23 ± 0.5 °C.

The influence of post-milling duration on the rheological behavior of fresh pastes was assessed using a rotational rheometer (Discovery HR-1, TA Instruments, USA). A four-bladed vane (height 42 mm, diameter 28 mm) together with a grooved cup (inner diameter 30.35 mm) served as the measurement geometry. To maintain a constant testing temperature of 23 ± 0.5 °C, approximately 70 g of fresh paste was poured into the cup, which was mounted within the fluid jacket of the instrument.

The shear protocol comprised the following steps: the paste was initially pre-sheared at a constant shear rate of 100 s^{-1} (per second) for 60 s (second) to eliminate the influence of any previous shear history. This was followed by a 30 s pause to allow structural equilibration. Subsequently, the shear rate was increased linearly from 0 to 120 s^{-1} over 90 s (up-curve) and then decreased back to 0 s^{-1} over a further 90 s (down-curve), with data recorded at every second during both phases. This shear protocol was selected based on our previous work measuring the rheology of blended cement with BOF slag [36]. The

Herschel–Bulkley (H-B) model (Eq. 4) was used to fit the down-curve data using the rheometer software (TRIOS, Discovery HR-1). Dynamic rheological properties were investigated at hydration times of 15, 30, 45, and 60 min, where the time count commenced at the moment cement and steel slag were brought into contact with water. To minimize water evaporation between measurements, the cup was covered with a metal lid during testing.

$$\tau = \tau_0 + k\gamma^n \tag{4}$$

where τ represents the shear stress (Pa), τ_0 denotes the yield stress (Pa), k is the consistency coefficient (Pa·s^n), and γ is the shear rate (s^{-1}) and n is the flow index. The compressive strength of hardened paste specimens (20 mm × 20 mm × 20 mm) was measured at 1, 7, and 28 days using a compression testing machine (Toni Technik, Germany) with a maximum capacity of 3000 kN (kilonewton) and a loading rate of 2.4 kN·s^{-1} (kilonewton per second). The mean of three replicates was reported as the compressive strength. To quantitatively evaluate the contribution of BOF and EAF slag to strength development, the Strength activation index (SAI) was calculated for each curing age, according to:

$$\mathrm{SAI} = \frac{\sigma_{\text{steel slag}}}{\sigma_{\mathrm{CRTL}}} \times 100 \tag{5}$$

where $\sigma_{\text{steel slag}}$ is the compressive strength of the slag-containing paste [MPa (megapascal)], and σ_{CRTL} is the compressive strength of the control paste (100% PC) at the same curing age (MPa).

The mineralogical composition of 28-day-hydrated paste samples was characterized by X-ray diffraction (XRD). Measurements were performed on back-loaded powder specimens using a PANalytical X'Pert Pro MPD diffractometer equipped with a rotating sample stage, operating in the 5–100° 2θ range. Co Kα radiation was employed at 45 kV (kilovolt) and 40 mA (milliampere), with data collected using a step size of 0.017° 2θ. Prior to analysis, hydration was stopped by immersing the specimens in isopropanol for 1 h, after which the liquid was decanted and replaced with fresh isopropanol for an additional 2 days. Following solvent exchange, the samples were oven-dried at 40 °C for 8 h to ensure complete drying. The dried material was then crushed in an agate mortar to a particle size below 63 µm. A 4 g portion of the sample was mixed with 1 g of calcium fluoride, used as an internal standard, and homogenized using a Thinky mixer for 10 min at 500 rpm (revolutions per minute). Hydration products were further characterized by TG/DTG analysis ("Characterization of Post-milled Steel Slag Powder" section), performed on < 63 µm powder obtained from the 28-day stopped-hydration paste specimens.

The leaching behavior of the cement–steel slag pastes was evaluated in accordance with the SFS-EN 12457–2 standard [42]. Paste specimens cured for 28 days were crushed and sieved to obtain particles smaller than 4 mm. The leaching procedure was carried out in sealed high-density polyethylene (HDPE) containers using deionized water at a liquid-to-solid mass ratio (L/S) of 10, with continuous agitation for 24 h at 23 ± 2 °C. At the end of the leaching period, the suspensions were filtered through 0.45 µm membrane filters to remove particulates and obtain clear eluates. The concentrations of leached elements were quantified by inductively coupled plasma–optical emission spectrometry (ICP-OES) using a Thermo Fisher Scientific iCAP 6500 Duo system. The leached amount of each constituent, normalized to the dry mass of the test portion, was calculated according to Eq. (6):

$$A_{10} = C_{10}\left(\frac{L_{10}}{M_D} + \frac{M_C}{100}\right) \tag{6}$$

where A_{10} shows the release of a constituent at L/S = 10 (mg·kg^{-1} (milligram per kilogram)), C_{10} is the concentration of the constituent in the eluate (mg·L^{-1} (milligram per liter)), L_{10} is the volume of leachant (L (liter)), M_{D} is the dry mass of the test portion [kg (kilogram)], and M_{C} is the moisture percentage of the dry mass.

Results and Discussion

Characteristics of Post-milled Steel Slag

Particle Size

The measured particle size distributions (PSD) of milled BOF and EAF slags at various post-milling durations are presented in Fig. 3. The PSD curves exhibit four prominent peaks whose magnitudes evolve with storage duration. The first and second peaks, located in the ranges 1–4 µm and 5–25 µm, respectively, decreased in intensity over time, indicating a reduction in the proportion of fine particles (< 25 µm) as post-milling duration increased. In contrast to the diminishing intensity of the finer fractions, the third and fourth peaks, located at approximately 50 µm and 100 µm, exhibited a pronounced increase in intensity over time. This trend became particularly pronounced after one year of storage, indicating a substantial degree of particle agglomeration, likely caused by the adhesion of fine particles to larger ones. Furthermore, the cumulative particle size distribution curves of both BOF and EAF slags shifted gradually to the right as the post-milling storage duration increased from short-term to long-term periods, reflecting a substantial increase in the overall particle size.

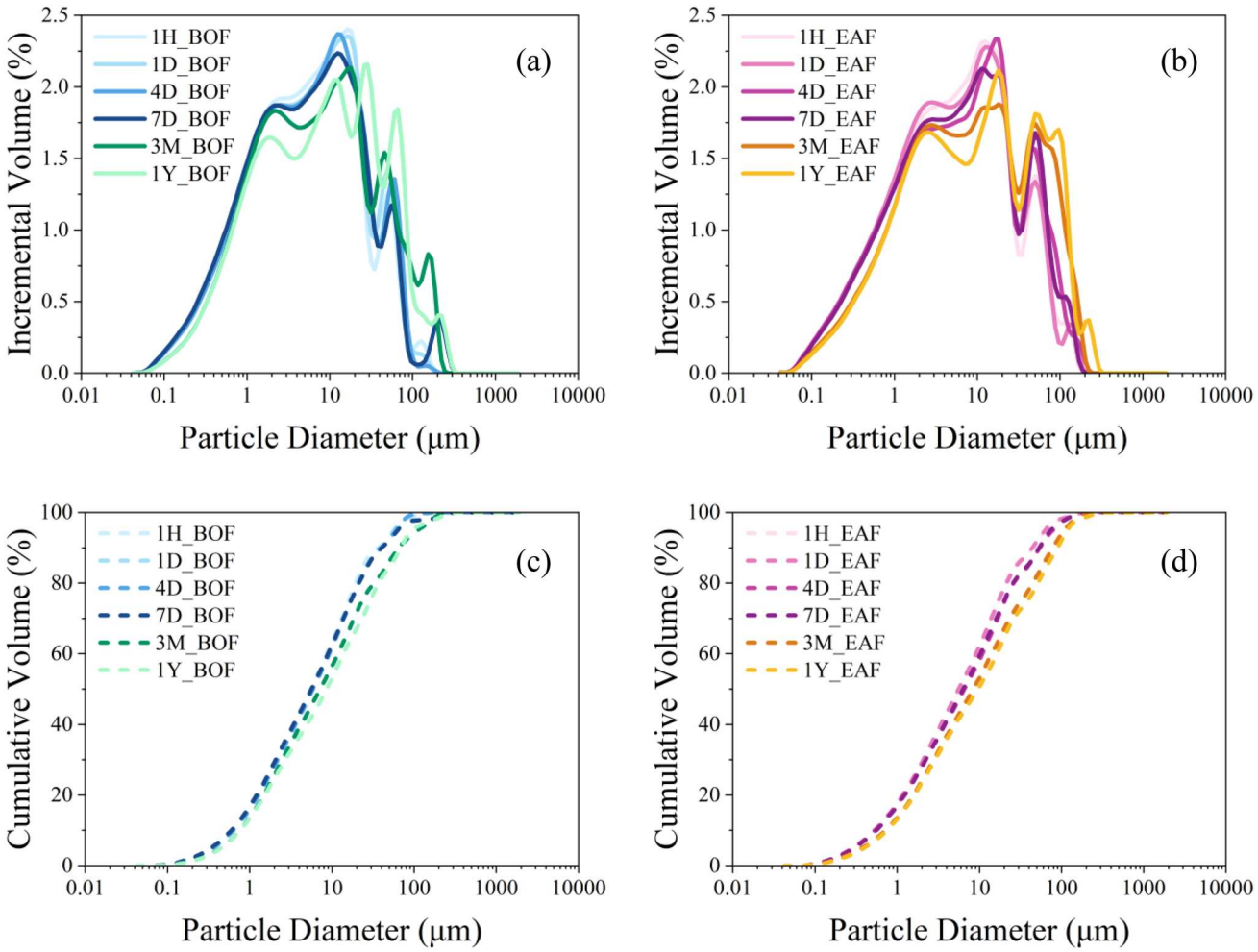

Fig. 3 Particle size distributions of milled BOF (**a**, **c**) and EAF (**b**, **d**) steel slags at different post-milling durations

Table 3 Particle size indicators of post-milled steel slags

	D_{10}		D_{50}		D_{90}		$(D_{90}-D_{10})/D_{50}$	D_{90}/D_{10}
	Value (μm)	SD (μm)	Value (μm)	SD (μm)	Value (μm)	SD (μm)		
1H_BOF	0.6	0.005	5.3	0.160	34.3	3.852	6.3	58.0
1D_BOF	0.6	0.008	5.5	0.115	37.8	2.796	6.8	63.7
4D_BOF	0.6	0.012	5.6	0.109	37.4	3.203	6.6	62.4
7D_BOF	0.6	0.009	5.4	0.567	40.3	13.661	7.3	71.1
3M_BOF	0.7	0.009	6.9	0.602	63.6	10.413	9.1	87.9
1Y_BOF	0.7	0.021	8.3	0.714	65.1	4.896	7.8	89.0
1H_EAF	0.5	0.010	5.6	0.268	41.8	4.328	7.4	83.4
1D_EAF	0.5	0.005	5.4	0.164	41.9	2.695	7.7	83.1
4D_EAF	0.5	0.005	6.3	0.267	51.8	2.822	8.2	102.0
7D_EAF	0.5	0.002	6.1	0.193	50.9	2.248	8.3	96.8
3M_EAF	0.7	0.004	8.0	0.666	74.3	5.154	9.1	109.0
1Y_EAF	0.7	0.032	9.3	1.791	84.5	13.730	9.0	118.5

As shown in Table 3, at 1 h after milling, D_{10} values were 0.6 μm for BOF slag and 0.5 μm for EAF slag, and remained nearly unchanged after 7 days. With prolonged storage, however, moderate increases were observed: after 3 months and 1 year, D_{10} rose to around 0.7 μm for BOF and EAF slag. Regarding the median size (D_{50}), minor variations were observed during the initial storage period. The D_{50} values increased slightly from 5.3 μm (BOF slag) and 5.6 μm (EAF slag) at 1 h to 5.6 μm and 6.3 μm after 4 days, indicating limited early agglomeration. However, the D_{50} values of 3M_BOF and 3M_EAF were significantly elevated, reaching 6.9 μm and 8.0 μm, corresponding to increases of 28% and 32% when compared with their 7-day counterparts. It should be noted that the largest D_{50} values were recorded after one year of storage, reaching 8.3 μm for BOF slag and 9.3 μm for EAF slag, representing increases of 56% and 67% relative to their initial (1H_BOF and 1H_EAF, respectively) values.

More pronounced changes were evident in the D_{90} values, which rose consistently with post-milling duration. From 1 h to 7 days, D_{90} increased by approximately 19% in both steel slag types, indicating noticeable agglomeration within the coarser fraction. When the post-milling duration was extended from 7 days to 3 months, the D_{90} of milled BOF slag and EAF slag increased from 40.3 μm to 63.6 μm and from 50.9 μm to 74.3 μm, respectively. However, after one year of storage, D_{90} increased markedly to 65.1 μm (1Y_BOF) and 84.46 μm (1Y_EAF). In addition to the shifts in characteristic particle sizes, the span $(D_{90}-D_{10})/D_{50}$, which reflects the relative width of the PSD, also increased progressively with storage time for BOF and EAF slags, indicating a broader and less uniform size distribution. The uniformity ratio D_{90}/D_{10}, representing the spread between the smallest and largest particle sizes, showed a more pronounced growth during storage. For BOF slag, it increased from 58.0 (1H_BOF) to nearly 90 after 1 year, while EAF slag exhibited an even larger rise from 83.4 to 118.5 over the same period.

The pronounced agglomeration reflected in the particle size changes of milled powders over extended post-milling durations can be attributed to the combined effects of electrostatic forces and residual moisture on particle surfaces. During milling, frequent collisions between particles and with the milling chamber can impart triboelectric charges to the powder particles. Specifically, particle breakage and frictional contact during milling cause electrons to transfer between surfaces, resulting in many particles acquiring net positive or negative charges. Because steel slag consists primarily of oxide minerals, which are electrically insulating, these charges cannot easily dissipate through conduction and instead remain on the particle surfaces. Once particles carry surface charges, electrostatic forces can directly induce agglomeration by pulling particles together. Oppositely charged particles attract one another through Coulombic forces, leading to clustering and the formation of agglomerates. Even particles with similar charges may attract through induced polarization, in which a charged particle induces a dipole in a nearby neutral or like-charged particle, generating a net attractive force at short range. As a result, charged powder particles tend to adhere upon contact, forming larger clusters [43]. While electrostatic attraction initiates and sustains particle clustering, residual moisture on the particle surfaces can further enhance agglomeration by forming liquid bridges at points of contact [44]. These two factors likely act synergistically: electrostatic forces bring particles into close proximity, and moisture bridges subsequently stabilize the agglomerates. This combined mechanism leads to the pronounced and persistent agglomeration observed during extended storage.

The powder morphology of milled BOF and EAF slags at 1 h and 1 year of post-milling storage was examined qualitatively using an optical microscope (DFC320, Leica), with representative images shown in Fig. 4. In the 1H_BOF and 1H_EAF samples, the powders contained small agglomerates that were randomly scattered throughout the sample rather than concentrated in specific regions. Such agglomerates typically arise during dry milling because of microcrack formation within particle structures, which generates electrostatic charges that promote the adhesion of fine particles onto larger ones [23]. In contrast, after prolonged storage (1Y_BOF and 1Y_EAF), the powders displayed extensive interconnection of these initial agglomerates, forming chain-like, compact structures. This morphological evolution is consistent with the PSD results, which revealed significant particle coarsening and pronounced agglomeration over extended storage duration.

Reactivity (R^3 Test)

The heat flow and cumulative heat release, normalized to the mass of steel slag, over 7 days are presented in Fig. 5. The initial peak, observed immediately after mixing the powders with the potassium solution, was attributed to the rapid wetting and alkali-driven dissolution of reactive phases of steel slag [37, 45]. At approximately 10 h, a peak was observed, corresponding to the precipitation of hydration products from the reaction between the steel slag and portlandite [37]. In the BOF slag series, this peak was barely visible, whereas in the EAF slag samples it was clearly distinguishable, indicating higher reactivity. Under R^3 test conditions, the alkaline environment provided by the potassium-based solution (KOH and K_2SO_4) can enhance the dissolution kinetics of reactive clinker-like phases present in the steel slags, which may include calcium silicate phases such as belite in BOF slag and belite and/or alite in EAF slag, while the added portlandite maintains a calcium-rich environment that promotes the rapid precipitation of calcium silicate hydrate

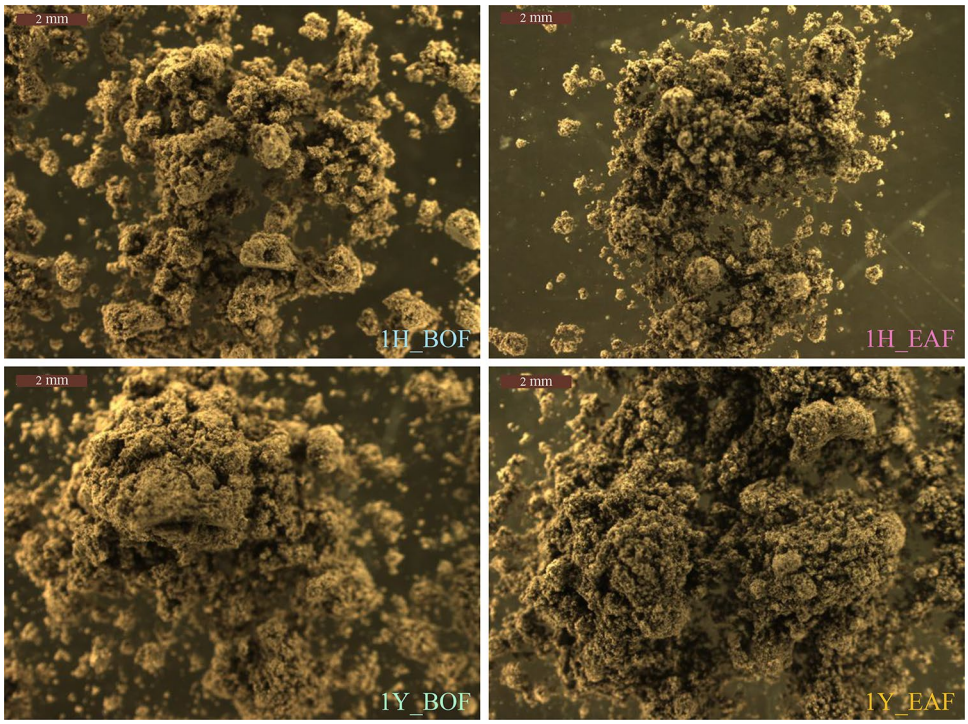

Fig. 4 Optical micrographs of BOF and EAF steel slags after 1 h (1H) and 1 year (1Y) post-milling storage

(C–S–H) from the dissolved silicate species [45–48]. In addition, if the steel slag releases alumina into the high-pH environment, it may react with the available sulfate ions to form ettringite. Moreover, since the R^3 mixture contains calcium carbonate, the dissolved alumina can also react with carbonate ions to form AFm phases such as monocarbonate or hemicarbonate [47]. With increasing post-milling storage time, from 7 days to 3 months and 1 year, the intensity of this peak declined markedly, which can be attributed to a reduction in the effective reactive surface area caused by the formation of stable agglomerates.

As shown in Fig. 5, all EAF slag samples released more heat than the BOF slag pastes across all post-milling storage durations. This difference can be attributed predominantly to their distinct mineralogical compositions. The presence of reactive phases in EAF slag, such as alite, brownmillerite, and mayenite, which were absent in BOF slag (Fig. 2), led to its higher reactivity.

In addition, the slightly higher CaO/SiO_2 ratio of EAF slag (1.23) relative to BOF slag (1.19) might indicate a greater abundance of reactive calcium-bearing phases, which in turn promote the formation of calcium silicate hydrates (C–S–H) and aluminum-substituted calcium silicate hydrates (C–A–S–H) [37, 47, 49].

The final emitted heat at 3 and 7 days for BOF slags stored for 1 h to 3 months ranged between 68–70 and 147–150 $J{\cdot}g^{-1}$ (joule per gram) SCM, respectively. These values are higher than the heat release of inert quartz (25 $J{\cdot}g^{-1}$ SCM at 7 days [50]), indicating that BOF slag exhibits measurable reactivity under the R^3 test conditions, consistent with previous findings by the authors [36]. The lowest values were recorded for BOF slag stored for one year, with 62 $J{\cdot}g^{-1}$ SCM at 3 days and 140 $J{\cdot}g^{-1}$ SCM at 7 days, highlighting the negative impact of extended post-milling storage. A similar trend was observed for EAF slags, as minor fluctuations in cumulative heat release were detected across different post-milling storage times up to 3 months. Based on the threshold reported by [51], EAF slag can be considered a moderately reactive material, with cumulative heat release values falling between 100 and 200 $J{\cdot}g^{-1}$ SCM. However, the 1Y_EAF samples exhibited the lowest reactivity, achieving only 120 $J{\cdot}g^{-1}$ SCM at 3 days and 150 $J{\cdot}g^{-1}$ SCM at 7 days.

These results suggest that in samples stored for up to 3 months, the agglomerates formed were relatively weak and could be broken down by effective dispersion techniques (using a high-shear blender during R^3 paste preparation), which limited their negative impact on reactivity. In contrast, the agglomerates formed after 1 year of storage appeared to be more stable and resistant to de-agglomeration, leaving a lasting negative effect on the reactivity of the steel slag. There were also significant variations in the relative increase in heat release between 3 and 7 days for BOF and EAF slags, reflecting differences in their chemical reactivity over time. The BOF slag series exhibited a higher Δ (H_{168}/H_{72}) of about 32%, compared with 20% for the EAF slag series. This difference is likely related to the higher content of reactive mineral phases in EAF slags, which accelerate hydration and lead to greater heat release. The higher Δ

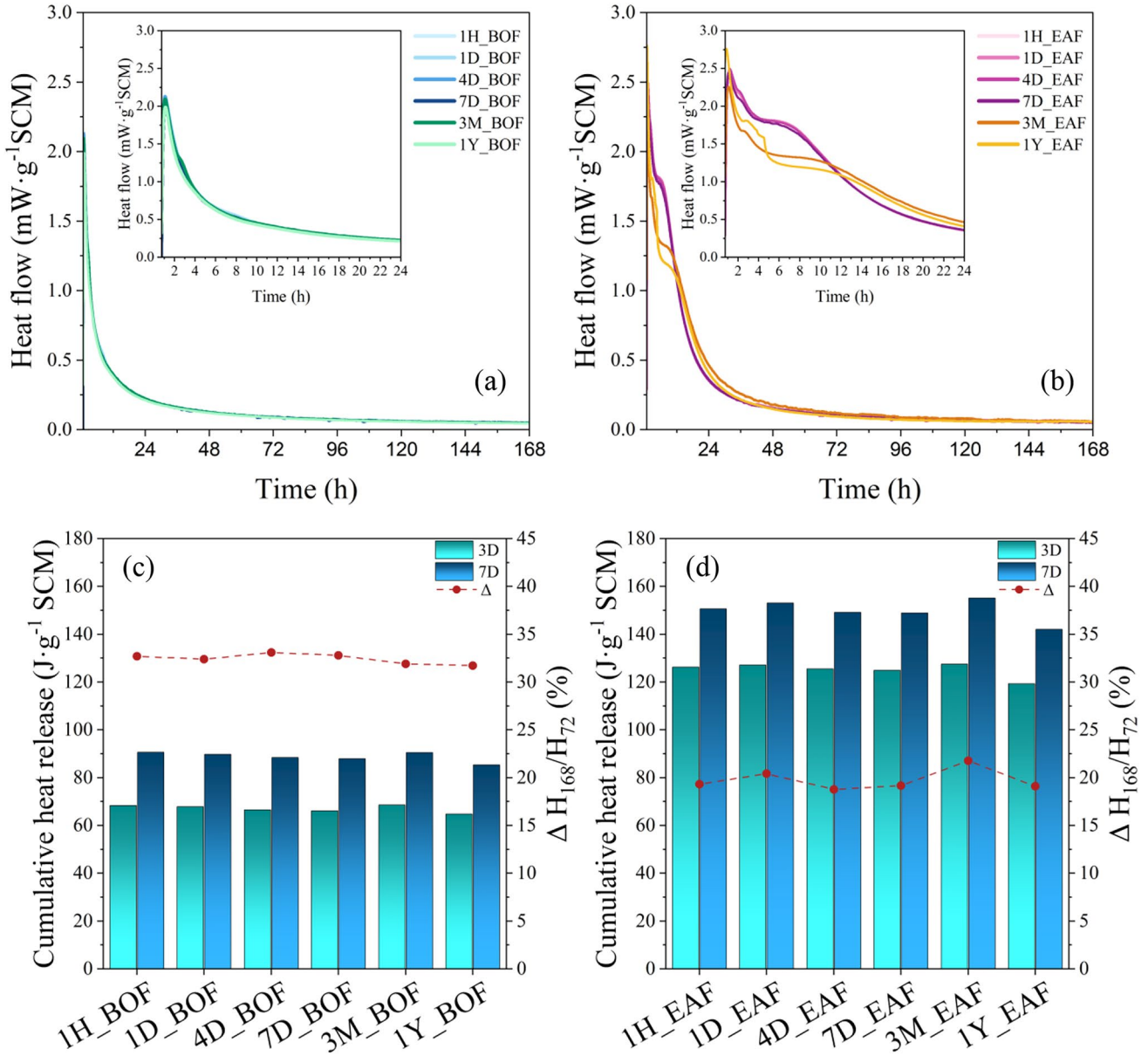

Fig. 5 Heat flow and cumulative heat release from the R^3 reactivity test of BOF (**a**, **c**) and EAF (**b**, **d**) steel slags as a function of post-milling duration

also suggests that, although BOF slag exhibits lower early reactivity, it may eventually reach similar total heat release values at later ages.

The TG/DTG profiles of the hydration-stopped pastes from the R^3 test after 7 days of curing at 40 °C are plotted in Fig. 6. A significant weight loss between 400 °C and 500 °C corresponds to the decomposition of portlandite in the pastes [52]. However, the decomposition temperature showed slight variations among samples, which can be attributed to factors such as fineness and crystallinity of the material [53]. The final amount of portlandite was then quantified using the tangential method, and the normalized portlandite consumption per gram of SCM (steel slag) is presented in Table 4. A good correlation was observed between portlandite consumption and cumulative heat release, consistent with the fact that heat release in the R^3 test is mainly governed by the reaction of calcium hydroxide with the silicate and aluminate phases of the steel slags [54].

According to the classification of supplementary cementitious materials proposed by [48, 55], materials with a cumulative heat release of less than 120 J·g^{-1} SCM and a calcium hydroxide consumption between 0 and 50 g per 100 g dried paste are regarded as slow-reacting or inert, whereas materials with a heat release of 120–750 J·g^{-1} SCM and a calcium

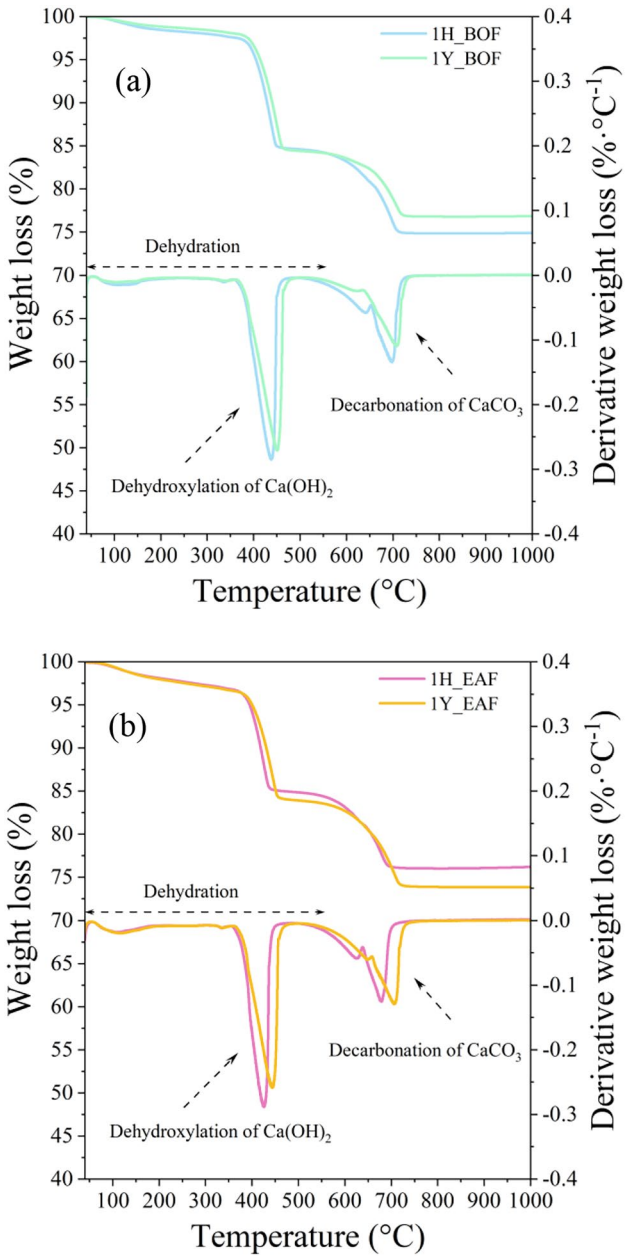

Fig. 6 Thermogravimetric (TG) and derivative (DTG) profiles of R^3 pastes prepared with BOF (**a**) and EAF (**b**) steel slags stored for 1 h (1H) and 1 year (1Y) after milling

hydroxide consumption of 40–180 g per 100 g dried paste are considered pozzolanic. Based on these thresholds, BOF and EAF slag can be classified as slow-reacting materials and moderately pozzolanic, respectively. It should also be noted that extended post-milling storage markedly reduced the portlandite consumption of both steel slags, confirming the negative influence of stabilized agglomeration formed after 1 year of storage on their reactivity.

Table 4 illustrates the bound water contents of the different mixes, calculated using Method A (furnace heating) and Method B (thermogravimetric analysis). A good correlation was observed between the two methods, in line with previous studies on R^3 bound water determination for common industrial SCMs such as fly ash and blast furnace slag [50, 56]. The highest bound water content (4.35 g per 100 g dried paste), confirming the formation of more extensive hydration products, was measured for 1H_EAF, but this value decreased to 3.43 g per 100 g dried paste for 1Y_EAF. A similar negative effect of extended post-milling storage was observed for BOF slag, where the bound water content dropped from 3.14 to 2.51 g per 100 g dried paste between 1H_BOF and 1Y_BOF. It is worth noting that the bound water values of BOF slag are only slightly higher than those reported for inert quartz (0.3–2.5 g per 100 g dried paste [40, 47, 57, 58]), further confirming its low reactivity.

Characteristics of Blended Cement

Hydration Heat

The heat flow and cumulative heat release profiles of the control cement (100% PC) and the cements containing 30% post-milled BOF and EAF slags are presented in Fig. 7. Regardless of steel slag type, replacing part of the cement with steel slag markedly reduced the cumulative heat release at 7 days, from 226 $J \cdot g^{-1}$ in the control sample (CC_CRTL) to approximately 189 $J \cdot g^{-1}$ and 160 $J \cdot g^{-1}$ in the systems blended with BOF and EAF slag, respectively. The negative impact of steel slag incorporation on hydration kinetics can also be observed in the heat flow curves, which show a significant reduction in the main thermal power peak occurring at around 10 h. This reduction is

Table 4 Portlandite (CH) consumption and bound water content

Mix ID	CH consumption g per 100 g SCM (SS)	Bound water (method A) g per 100 dry past	Bound water (method B) g per 100 dry past
1H_BOF	24.87	3.14	3.83
1H_EAF	49.46	4.35	4.87
1Y_BOF	9.02	2.51	3.05
1Y_EAF	26.73	3.43	4.79

Method A (furnace heating); Method B (thermogravimetric analysis)

SS steel slag

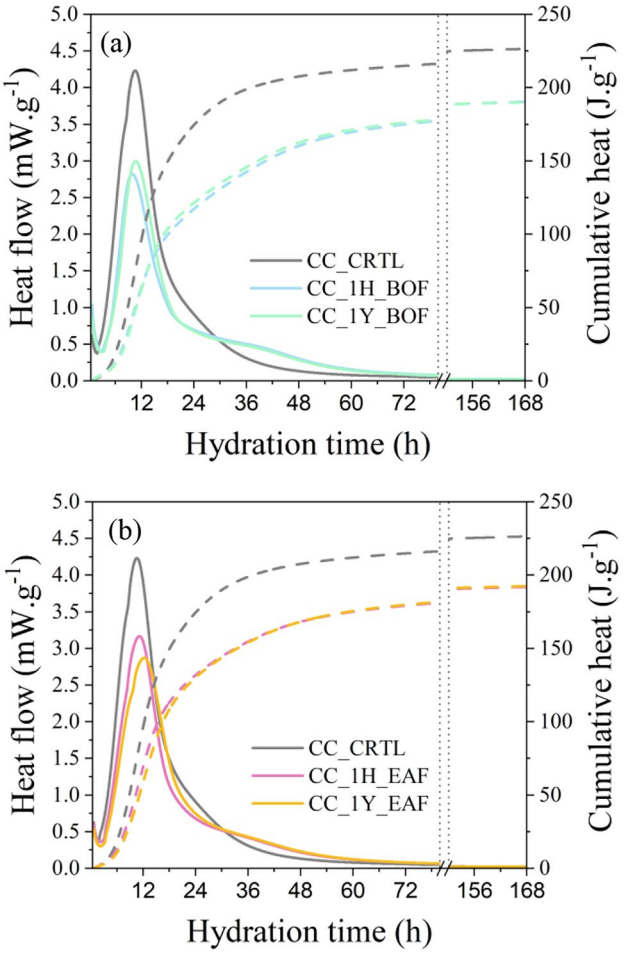

Fig. 7 Heat flow and cumulative heat release curves of cement pastes containing 30% BOF (**a**) or EAF (**b**) slag stored for 1 h (1H) and 1 year (1Y) after milling, along with the reference cement (CC_CRTL)

attributed to the lower hydraulic reactivity of steel slag, associated with its crystalline structure and non-hydraulic Fe-bearing phases, and is consistent with previous research findings [59–62].

The influence of post-milling storage was relatively minor. Long-term storage (1 year) produced a slight right-shift of the main peak relative to short-term storage (1 h), suggesting a modest delay in the nucleation and growth of C–S–H and portlandite. This delay may arise from increased particle agglomeration, which limits water accessibility to fresh slag surfaces and ultimately reduces the availability of Ca^{2+} needed to reach saturation before further hydration of the slag can proceed [63–65]. Nevertheless, these effects diminished over hydration time: while CC_1H_BOF and CC_1H_EAF released approximately 122 and 132 $J{\cdot}g^{-1}$ within the first 24 h (compared to 117 and 130 $J{\cdot}g^{-1}$ for 1Y_BOF and 1Y_EAF), the cumulative heat of the 1-year-stored slags approached that of the fresh slags by 7 days, indicating that the agglomerated particles ultimately became available for hydration at later ages.

Between the two steel slag types, the EAF-blended cements consistently exhibited slightly higher heat evolution peak intensities during the acceleration period and maintained higher cumulative heat release values throughout the 7-day hydration period compared with the BOF-blended counterparts. This persistent divergence agrees with the R^3 results, reflecting the higher activity of EAF slag, which can be attributed to its greater availability of reactive silicate and aluminate phases.

Rheological Behavior

The rheological behavior of the reference cement paste and the blended systems incorporating steel slag stored for different durations (1 h and 1 year) are presented in Fig. 8. As anticipated, the viscosity of all pastes decreased with increasing shear rate, a manifestation of shear-thinning behavior that can be ascribed to the disruption of the flocculated particle network, wherein the rate of structural breakdown predominates over the tendency for re-agglomeration under the imposed shear field [66]. As evident from the shear stress–shear rate curves (Fig. 8), partial replacement of cement with steel slag (both BOF and EAF slag) shifted the flow curves downward, indicating reduced shear stress at equivalent shear rates. The reduction in shear resistance can be ascribed to the lower reactivity of steel slag, which limits the extent of early hydrate formation within the system and consequently delays network stiffening, ultimately yielding a more fluid paste [67].

Figure 9 illustrates the evolution of the apparent viscosity, defined herein as the ratio of shear stress to shear rate at a reference shear rate of 20 s^{-1}, together with the yield stress, determined through fitting to the Herschel–Bulkley model, for the cement pastes monitored at hydration times of 15, 30, 45, and 60 min following the commencement of powder–water interaction. All mixtures displayed a clear time-dependent rheological response, with the progression of hydration giving rise to steadily increasing apparent viscosity and yield stress. In the case of the reference paste (CC_CRTL), a gradual build-up in apparent viscosity was evident, rising from 6.9 Pa·s at 15 min to 8.9 Pa·s at 60 min; the yield stress evolved in a parallel manner. This time-dependent stiffening can be attributed to the continuous formation of hydration products, which increase frictional interactions within the mixture [68–70].

Post-milling duration exerted a negative influence on the dynamic rheological characteristics of the blended cement pastes. Steel slags subjected to long-term storage (1 year) exhibited consistently lower yield stress and apparent viscosity than their freshly milled counterparts (1 h) across all hydration times. For instance, at 15 min, yield stress

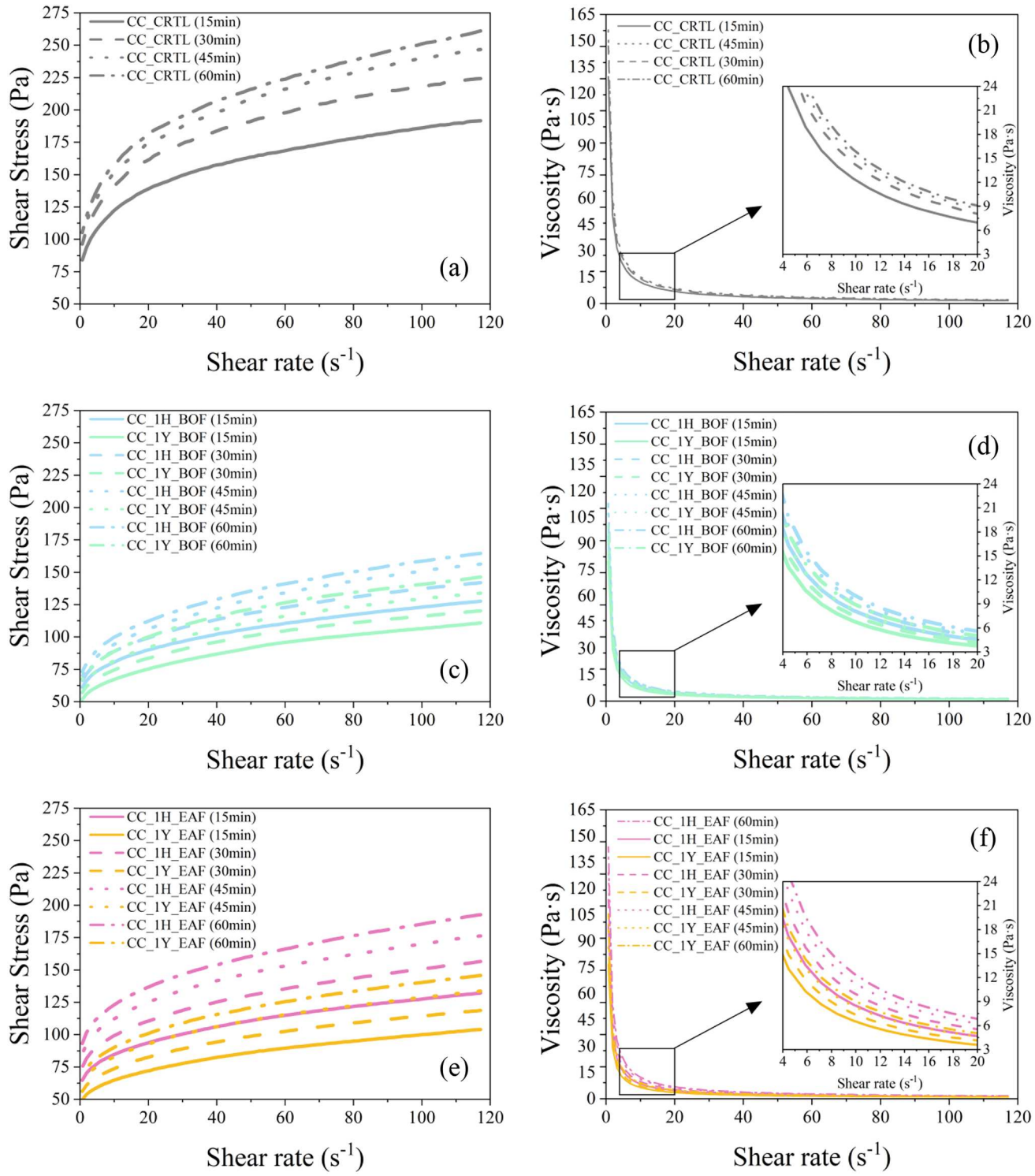

Fig. 8 Dynamic shear stress/viscosity-shear rate of paste composites after different resting times (15–60 min)

decreased by 14% (49.2 → 42.3 Pa) and apparent viscosity by 16% (4.4 → 3.7 Pa·s) when comparing CC_1H_BOF with CC_1Y_BOF. Similarly, CC_1Y_EAF showed reductions of 22% in yield stress (53.5 → 41.6 Pa) and 23% in apparent viscosity (4.6 → 3.6 Pa·s) relative to CC-1H_EAF. This behavior could be attributed to the high degree of stabilized agglomeration generated during extended post-milling storage, which reduced the effective contact area between slag

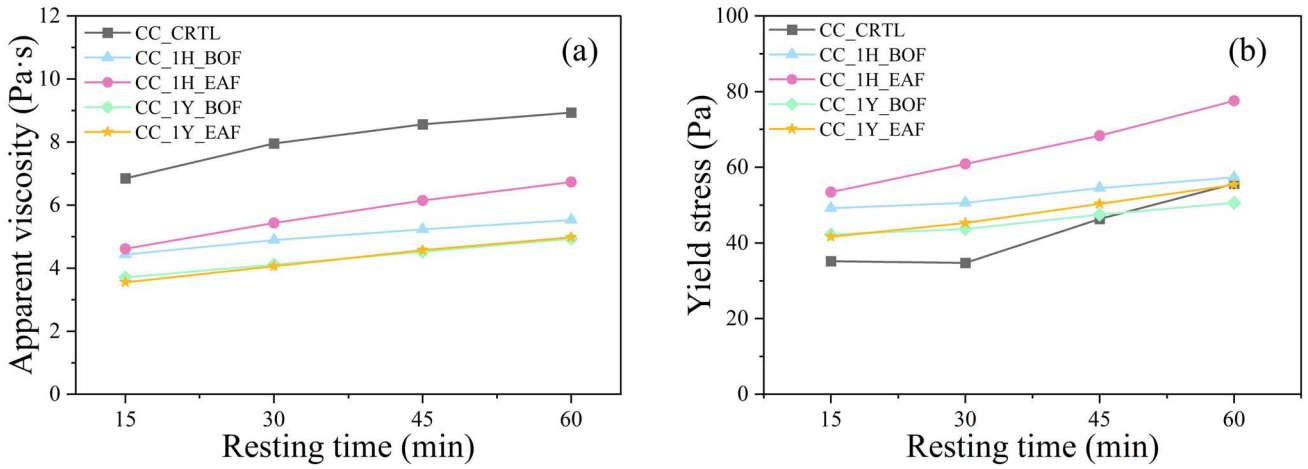

Fig. 9 Time-dependent apparent viscosity (**a**) and yield stress (**b**) of paste composites

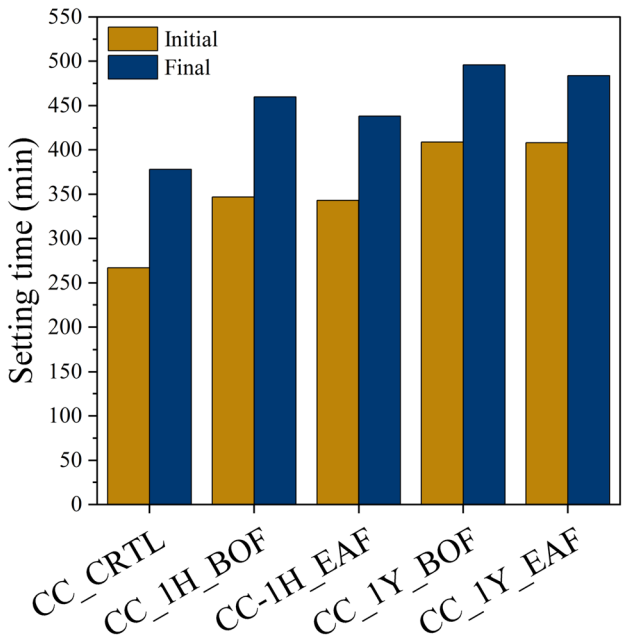

Fig. 10 Initial and final setting times of cement pastes

particles and water, increased the proportion of free water in the mixture, and ultimately produced a less viscous paste while hindering the rate of structuration [71, 72].

Clear differences between EAF- and BOF-blended pastes were also evident. At all hydration times, the EAF-blended pastes consistently developed higher yield stress and apparent viscosity than the BOF-blended counterparts. At 60 min, the CC_1H_EAF paste exhibited a yield stress of 77.6 Pa and an apparent viscosity of 6.7 Pa·s, while CC_1H_BOF showed values of 57.3 Pa and 5.5 Pa·s. This superior rheological performance of the EAF-containing blends correlates with the higher intrinsic reactivity of EAF slag, as revealed by the R^3 tests and further confirmed by the calorimetric assessment of hydration kinetics, which promotes greater early formation of hydration products and consequently stronger interparticle bonding.

Setting Time

The setting times of the pastes are presented in Fig. 10. Replacing 30% of cement with steel slag resulted in a noticeable prolongation of both the initial and final setting times relative to the control cement paste. This retarding effect of steel slag, attributable to the inhibition of nucleation and growth of hydration products (C–S–H and portlandite), is consistent with existing studies [73–76].

Among the blends, CC_1H_EAF displayed the shortest setting times, with an initial and final set of 343 min and 438 min, respectively. However, when one-year post-milled EAF slag (1Y_EAF) was incorporated, the setting times increased to 408 min and 484 min, indicating a significant retardation. A similar trend was observed for BOF slag: the 1Y_BOF mixture reached initial and final setting times of 409 min and 496 min, which were slightly longer than those recorded for CC_1H_BOF (347 min and 460 min, respectively). This retardation is consistent with the calorimetry results (Fig. 7), which showed a shift of the main hydration peak toward longer times in the 1-year post-milled slag systems, attributable to the high degree of particle agglomeration. A clear correlation was also observed with the R^3 reactivity test: EAF slag, which exhibited higher reactivity than BOF slag in the R^3 method, evidenced by greater cumulative heat release, higher bound water content, and increased portlandite consumption, correspondingly produced shorter setting times in the blended cement systems.

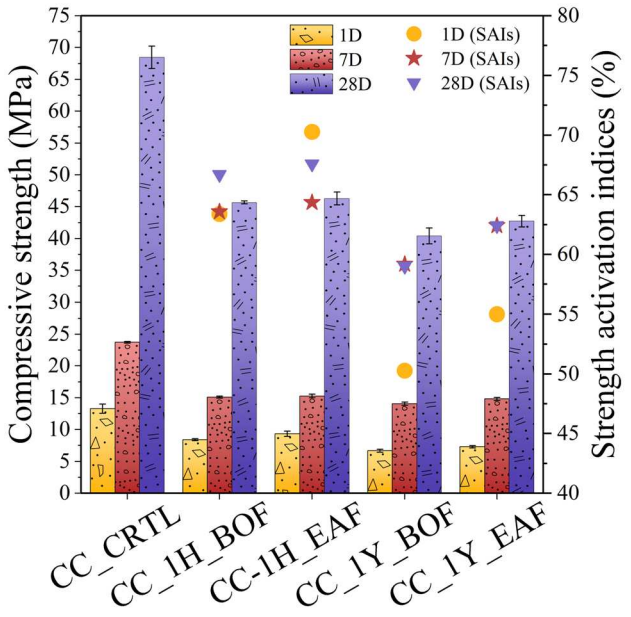

Fig. 11 Compressive strength and corresponding strength activity indices (SAIs) of paste specimens at 1, 7, and 28 days of curing

Compressive Strength

The compressive strengths of the cement composites at 1, 7, and 28 days (average of three replicate samples) are presented in Fig. 11. Independent of steel slag type and post-milling duration, all steel slag-blended systems exhibited lower strength than the control paste (CC_CRTL), whose strengths were 13.3 ± 0.7 MPa, 23.7 ± 0.1 MPa, and 68.5 ± 1.8 MPa at 1, 7, and 28 days, respectively. These results comply with the SFS-EN 197–1 [77]specification for CEM I 52.5 N (> 52.5 MPa at 28 days) and are consistent with the compressive strength range reported by the Pika Cement datasheet (57–68 MPa; Finnsementti, Finland) [78]. At 1 day, CC_1H_BOF and CC_1H_EAF attained compressive strengths of 8.4 ± 0.2 MPa and 9.3 ± 0.4 MPa, respectively, whereas their long-stored counterparts (CC_1Y_BOF and CC_1Y_EAF) developed only 6.7 ± 0.3 MPa and 7.3 ± 0.2 MPa. The 16–17% enhancement in early strength observed in systems with freshly milled steel slags (1 h) could be ascribed to their lower degree of agglomeration, which increases the availability of reactive surface area during the initial stages of hydration.

At 7 days, the same trend was observed, with CC_1H_BOF and CC_1H_EAF reaching 15.1 ± 0.2 MPa and 15.3 ± 0.3 MPa, compared with 14.0 ± 0.3 MPa and 14.8 ± 0.2 MPa for the corresponding 1-year samples. However, the relative differences between 1H and 1Y steel slag blends were reduced to less than 8%. By 28 days, the strengths of all steel slag-blended systems converged to similar levels: 45.7 ± 0.2 MPa (CC_1H_BOF), 46.3 ± 1.0 MPa (CC_1H_EAF), 40.4 ± 1.3 MPa (CC_1Y_BOF), and 42.7 ± 0.9 MPa (CC_1Y_EAF). The difference between short-term (1 h) and long-term (1 year) post-milled steel slags diminished to only 2–3%, within the range of experimental deviation, indicating no statistically significant impact of post-milling storage on 28-day compressive strength.

The calculated SAIs further clarify the influence of post-milling storage: freshly milled slags (1H) exhibited notably higher SAIs than their 1Y counterparts for strength at 1 day, with differences of approximately 13–20 percentage points depending on slag type. By strength at 28 days, this disparity diminished to below 8%, demonstrating that the adverse effect of long-term agglomeration is largely restricted to early hydration. The consistently higher SAIs of the EAF-based system additionally reflected its greater reactivity.

These findings align with the calorimetry results (Fig. 7), which showed that the initial disparity in cumulative heat release between freshly milled and long-stored steel slags was progressively compensated at later hydration stages. This suggests that the negative influence of agglomeration is predominantly an early age effect, and with sufficient curing time, hydration reactions proceed to comparable extents regardless of storage conditions. It should be noted that a slight but consistent superiority of EAF slag over BOF slag was observed at all curing ages, reflecting its higher intrinsic reactivity, in agreement with the R^3 reactivity test results.

Phase Assemblage

The TG/DTG profiles of the blended pastes at 28 days (Fig. 12) display three main weight loss regions. The first weight loss, occurring between 50 and 120 °C, is related to the dehydration of C–S–H gel and decomposition of ettringite [52]. Substitution of cement with steel slag, irrespective of slag type or storage condition, led to a reduction in this weight loss, reflecting the lower formation of C–S–H and ettringite phases in agreement with the limited hydraulic reactivity of steel slag observed in the R^3 test. Introducing the freshly milled slag (CC_1H_BOF) promoted greater formation of C–S–H and ettringite compared with the long-stored slag (CC_1Y_BOF), consistent with the higher effective surface area of 1H_BOF slag. In the case of EAF slag, no significant variation was detected in this region; however, the decomposition peak associated with AFm phases at ~ 180 °C [52] was slightly reduced with increasing post-milling storage time.

The second major weight loss, observed between ~ 400 and 500 °C [52], corresponds to the dehydroxylation of portlandite. Among the mixes, the pure cement paste (CC_CRTL) exhibited the highest weight loss, followed by the EAF slag–cement and then the BOF slag–cement pastes, consistent with differences in hydration kinetics. A further

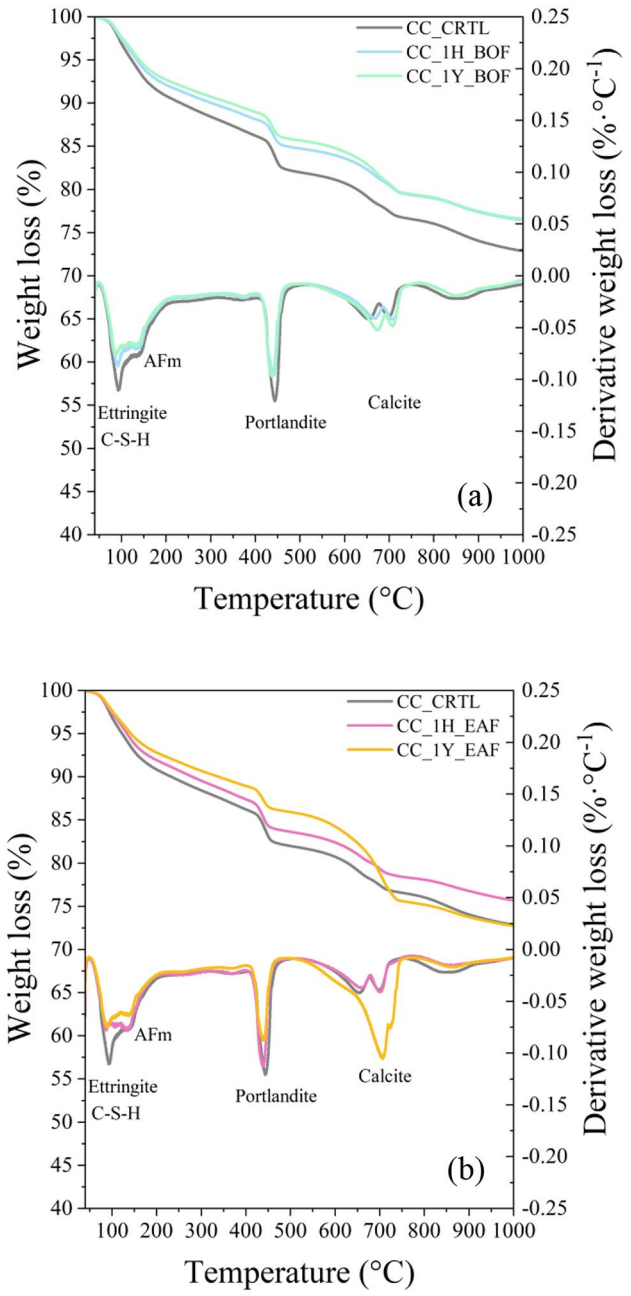

Fig. 12 Thermogravimetric (TG) and derivative (DTG) curves of 28-day cement pastes with 30% BOF (**a**) or EAF (**b**) slag stored for 1 h and 1 year after milling

distinction was observed between CC_1H_EAF and the blend containing 1Y_EAF, with CC_1Y_EAF exhibiting a smaller portlandite peak. This suggests that prolonged post-milling storage reduced the reactivity of the slag and limited its contribution to hydration. The third principal weight loss, detected between ~ 600 and 750 °C, is attributed to calcite ($CaCO_3$) decomposition [49]. Only minor amounts of calcite were found in the control paste and the blends with freshly milled slags (CC_1H_BOF, CC_1H_EAF). In contrast, pastes incorporating long-stored slags, especially CC_1Y_EAF, exhibited larger calcite-related mass losses.

Notably, the chemically bound water content, estimated from the mass loss between 40 and 550 °C [79], decreased when 30% of cement was replaced by steel slag. This parameter, which is often used as an indicator of hydration degree and strength development [80], declined from 16.8% in CC_1H_EAF to 14.6% in CC_1Y_EAF. A similar reduction trend was observed in BOF slag–cement pastes, from 15.7% to 14.8% as the storage period increased from 1 h to 1 year. These results are consistent with the lower reactivity predicted by the R^3 test and with the compressive strength performance of the pastes.

To obtain more detailed information on the hydrated products of the blended system, X-ray diffraction (XRD) was performed. The results of the Rietveld quantitative phase analysis of the 28-day samples are summarized in Table 5. All pastes exhibited the same phase assemblage, comprising five principal hydration products: portlandite, ettringite, AFm (reported here as hemicarbonate), calcite, and a substantial amorphous fraction attributed to C–S–H/C–A–S–H. Consistent with the literature, steel slag substitution exerted a limited effect on hydration products, changing their proportions rather than their types [81, 82].

Relative to the control paste (16.08 wt%), portlandite decreased by 29% to 11.40 wt% (CC_1H_BOF), 16% to 13.50 wt% (CC_1H_EAF), 29% to 11.43 wt% (CC_1Y_BOF), and 24% to 12.28 wt% (CC_1Y_EAF). This reduction was primarily attributable to dilution from slag substitution and became more pronounced in blends incorporating one-year post-milled slag, where agglomeration further suppressed reactivity. The trend was consistent with the TG/DTG results (Fig. 12), which showed a smaller portlandite dehydroxylation peak at 400–500 °C. Ettringite remained stable at ~ 5.4–6.3 wt%, indicating an adequate sulfate balance at 28 days [83, 84]. AFm (quantified here as hemicarbonate) was lower in the slag blends than in the control (decreasing from 3.37 wt% to 1.65–2.78 wt%), as expected given the reduced effective C_3A supply and possible AFm polymorph interconversion; note that a small portion of AFm may have been present as monocarbonate but modeled as hemicarbonate within the refinement constraints [83, 85, 86].

At 28 days, the crystalline phases of steel slag were consumed to varying extents in the cement mixture, and residual unhydrated phases reflected the steel slag type. For instance, gehlenite appeared mainly in the BOF pastes (up to 2.81 wt%), whereas mayenite was characteristic of the EAF pastes (1.80–2.34 wt%). The 28-day phase assemblage of blended cements showed limited sensitivity to the storage history of steel slag. BOF pastes showed only modest differences between 1 h and 1 year, whereas CC_1Y_EAF contained substantially more unreacted akermanite (14.33 vs

Table 5 Results of Rietveld qualitative phase analysis of 28-day cement composites

Phases	Formula	CC_CRTL	CC_1H_BOF	CC_1H_EAF	CC_1Y_BOF	CC_1Y_EAF
Alite(M3)	Ca_3SiO_5	2.1	0.3	0.5	4.2	0.0
Alite (M1)	Ca_3SiO_5	11.2	11.4	8.9	7.8	5.3
Belite (β)	Ca_2SiO_4	6.1	3.0	3.9	3.4	4.4
Brownmillerite	$Ca_2(Al,Fe)_2O_5$	3.7	4.1	4.5	2.9	5.7
Calcite	$CaCO_3$	7.8	6.1	5.7	6.4	5.7
Quartz	SiO_2	0.3	0.9	0.0	1.5	1.2
Gehlenite	$Ca_2Al(AlSiO_7)$	0.0	2.8	1.5	2.8	0.0
Bredigite	$Ca_7Mg(SiO_4)_4$	0.0	0.0	0.3	0.0	0.1
Mayenite	$Ca_{12}Al_{14}O_{33}$	0.0	0.0	1.8	0.0	2.3
Akermanite	$Ca_2MgSi_2O_7$	0.0	6.1	7.2	6.3	14.3
Wustite	FeO	0.0	1.8	2.3	0.1	1.9
Periclase	MgO	0.8	0.3	0.9	1.0	0.9
Portlandite	$Ca(OH)_2$	16.1	11.4	13.5	11.4	12.3
Ettringite	$Ca_6Al_2(SO_4)_3(OH)_{12}\cdot 26H_2O$	6.3	5.5	5.4	5.4	5.8
Hemicarbonate	$Ca_4Al_2O_6(CO_3)_{0.5}\cdot 12H_2O$	3.4	2.5	1.7	2.8	2.6
Amorphous	–	64.9	62.2	62.4	61.1	54.1

7.20 wt%) and a markedly lower amorphous fraction (54.09 vs 62.42 wt%) than CC_1H_EAF, indicating suppressed dissolution and hydrate formation after prolonged post-milling time, likely due to agglomeration that reduced the effective reactive surface area.

Leaching

The leaching results are summarized in Table 6. Although the incorporation of BOF and EAF slags introduced trace metals that are largely absent in Portland cement, most heavy metals remained strongly immobilized within the cementitious matrix. Under highly alkaline pore solution conditions, hydration products such as C–S–H, ettringite, and AFm phases effectively restrict the mobility of trace elements [87]. For instance, Ahmad et al. [88] reported that in BOF slag composites, vanadium was immobilized within hydration products: during C_2S hydration, C–S–H incorporates V_2O_5 through substitution of V in the tetrahedral Si site, thereby reducing its leachability.

To assess the environmental acceptability of the steel slag–blended binders, their leaching behavior was evaluated with reference to the principal European and international regulatory frameworks governing cementitious materials and related secondary resources. In Europe, environmental performance is governed by the Construction Products Regulation [89] and supported by both EU-level and national instruments, including the EU Waste Acceptance Criteria (WAC) [90], Finnish environmental regulations for construction materials (MARA decree 843/2017) [91], the German Ersatzbaustoffverordnung (EBV) [92], and the Dutch Soil Quality Decree [93].

The ICP–OES results indicated that the leaching concentrations of metals from all mixtures were below the thresholds prescribed for construction materials in these frameworks, with the exception of barium in BOF slag blends.

Table 6 Leachate concentrations ($mg\cdot kg^{-1}$) of control and steel slag–cement composites

	pH	As	Ba	Cd	Cr	Cu	Mo	Ni	Pb	Sb	V	Zn	Mn	Ti	P
CC_1H_BOF	12.49	< 0.01	36	< 0.002	< 0.01	0.023	0.15	< 0.01	0.043	< 0.01	< 0.01	< 0.04	< 0.04	< 0.15	< 0.5
CC_1H_EAF	12.51	< 0.01	19	< 0.002	< 0.01	0.018	0.1	< 0.01	0.056	< 0.01	< 0.01	< 0.04	< 0.04	< 0.15	< 0.5
CC_1Y_BOF	12.51	< 0.01	34	< 0.002	< 0.01	0.03	0.15	< 0.01	0.036	< 0.01	< 0.01	< 0.04	< 0.04	< 0.15	< 0.5
CC_1Y_EAF	12.48	< 0.01	20	< 0.002	< 0.01	0.027	0.11	< 0.01	0.044	< 0.01	< 0.01	< 0.04	< 0.04	< 0.15	< 0.5
CC_CRTL	12.54	< 0.01	15	< 0.002	0.015	0.016	0.11	< 0.01	0.027	< 0.01	< 0.01	< 0.04	< 0.04	< 0.15	< 0.5
EU WAC_I	–	0.5	20	0.04	0.5	2	0.5	0.4	0.5	0.06	–	4.0	–	–	–
Eu WAC_N	–	2	100	1	10	50	10	10	10	0.7	–	50	–	–	–

EU WAC_I and EU WAC_N correspond to the EU waste acceptance criteria (Council Decision 2003/33/EC) for inert waste (I) and non-hazardous waste (N)

The BOF slag mixtures released 34–36 mg·kg^{-1} Ba, slightly above the inert threshold of 20 mg·kg^{-1} yet remaining well below the non-hazardous WAC limit (100 mg·kg^{-1}). Barium in steel slags is commonly hosted in solid solutions with calcium phases, such as gehlenite, or dispersed within the glassy matrix [94–96]. Under strongly alkaline conditions (pH ≈ 12), these reservoirs can liberate Ba^{2+} into solution [97, 98], explaining the elevated, yet moderate, concentrations observed. Beyond Europe, the environmental performance of the binders was evaluated against international frameworks. According to the U.S. EPA Toxicity Characteristic Leaching Procedure (TCLP) [99], the regulatory thresholds for Pb (5 mg·L^{-1}) and Ba (100 mg·L^{-1}) indicate that all mixtures can be classified as non-hazardous with wide safety margins. In Asia, the Japanese Industrial Standards (JIS) A 5011 [100] and A 6206 [101] specify environmental quality criteria for slag aggregates and ground granulated blast furnace slag, defining leaching limits typically between 0.01 and 0.05 mg·L^{-1} for Cd, Pb, and Cr (VI). The measured concentrations in this study were substantially below these limits, confirming that the steel slag–blended binders comply with the most stringent product-level environmental standards currently in use worldwide.

A comparison between freshly milled slags (1 h) and slags stored for one year prior to use (1 year) revealed that storage did not systematically alter leaching behavior. For both BOF and EAF slag-containing samples, long-term storage slightly increased Cu release but slightly reduced Pb concentrations. These fluctuations may be explained by two mechanisms: (i) storage-induced agglomeration, which decreases slag reactivity and reduces the formation of new hydrates capable of binding metals; and (ii) in the short-term stored powders, a lower degree of agglomeration may have provided a larger effective contact surface with the leachant, ultimately facilitating the release of surface-associated metals [102].

Conclusions

This study delineated how post-milling duration, the storage interval between milling and use in cement composites, shapes the characteristics of milled powders and their performance as SCMs. BOF and EAF slags were milled under identical conditions and subsequently stored for 1 h, 1 day, 4 days, 7 days, 3 months, and 1 year in a controlled environment. The time-dependent changes in the powders were investigated through particle size analysis and reactivity quantification using the R^3 test. To bridge the storage-induced changes with practical performance, cement was partially substituted with steel slags stored for 1 h and 1 year, and the blended composites were investigated with respect to setting time, rheological behavior, hydration kinetics, compressive strength, and hydration product assemblage, alongside leaching performance to address environmental aspects.

- The particle size analysis revealed that prolonged post-milling storage-induced substantial coarsening of milled steel slags. Quantitatively, the D_{50} values of BOF and EAF slags increased by 56% and 67%, respectively, after one year of storage compared with their freshly milled counterparts (1 h), while even greater increases were observed in the D_{90} fraction, reflecting the formation of stabilized, chain-like agglomerates.
- Although the cumulative heat release showed only minor fluctuations during short-term post-milling (up to 3 months), one year of storage led to slight but measurable reductions for both steel slag types, reflecting the detrimental effect of stable agglomerates that resisted dispersion. The R^3 test further revealed the low reactivity of BOF slag, with heat release values only slightly higher than inert quartz, whereas EAF slag consistently fell within the range of moderately reactive SCMs.
- Thermogravimetric analysis confirmed a consistent correlation between portlandite consumption, bound water content, and cumulative heat release in the R^3 system. Extended post-milling storage (1 year) led to subtle reductions in both portlandite consumption and bound water compared with freshly milled slags (1 h), highlighting the negative influence of stabilized agglomeration on the extent of hydration.
- Calorimetry results showed that slag incorporation reduced the intensity of the main hydration peak and the cumulative heat release; however, the influence of post-milling duration was relatively minor. One year of storage caused a slight delay in the main peak and a modest reduction in cumulative heat release, particularly at early ages. EAF-blended cements consistently exhibited greater heat release than BOF composites, in line with the higher reactivity of EAF slag confirmed by the R^3 tests.
- The dynamic rheological response of steel slag–blended pastes was influenced by post-milling duration: long-term storage (1 year) produced less viscous pastes due to a greater amount of free water associated with the high degree of agglomeration. In parallel, compared with BOF-containing systems, EAF blends consistently developed stronger interparticle networks, a behavior attributable to their higher intrinsic reactivity and the consequent acceleration of early hydrate formation.
- Partial replacement of cement with steel slag was found to extend the initial and final setting times relative to the control paste, an effect that became slightly pronounced when one-year post-milled steel slag was used, since the

agglomerations formed during prolonged storage delays further hindered the onset of hydration.

- Freshly milled steel slags (1 h) developed higher early age compressive strengths than one-year-stored steel slags (1 year), in agreement with the higher reactivity observed in the R^3 tests. However, this difference diminished with hydration time, and by 28 days the strengths of the 1 h and 1-year post-milled slags had converged, indicating that the negative influence of agglomeration is confined to the early stages of hydration.
- Thermogravimetric and XRD analyses revealed that freshly milled slags contributed more effectively to the formation of hydration products such as portlandite, while one-year post-milled slags retained a higher proportion of unreacted crystalline phases such as akermenite.
- Leaching tests revealed that post-milling storage had no systematic effect on leaching behavior, confirming that heavy metals remained largely immobilized within the cementitious matrix.

Recommendations and Future Work

Overall, extended post-milling duration altered powder characteristics, leading to a slight but measurable negative influence on the performance of steel slag as an SCM, particularly at early ages. To preserve the full potential of this metallurgical residue and enable its large-scale valorization in the cement industry, minimizing the time period between milling and use is recommended. In industrial practice, this may require producing smaller batches and using the milled slag within a limited time frame rather than storing it for prolonged periods.

Nevertheless, further research is required to clarify how different storage environments, particularly variations in humidity and temperature, affect the milled powders. The possibility that certain mineralogical changes, such as oxidation of Fe-bearing phases or the gradual modification of minor constituents, may occur during storage also merits careful examination. At present, it is unclear whether such changes would intensify the loss of reactivity associated with agglomeration or partially counterbalance it. The use of grinding aids represents another avenue worth exploring, especially as a means to inhibit agglomeration during storage. However, their long-term effectiveness, and any unintended interactions with slag chemistry, remain to be established through controlled studies. Looking ahead, adopting a statistical experimental design, such as ANOVA-based methodologies, would provide a more rigorous framework for quantifying experimental uncertainty, identifying interactions among key variables (slag type, milling intensity, storage duration, environmental conditions), and ultimately strengthening the reliability and general applicability of future findings.

Acknowledgements This work has received funding from the European Union's Horizon Europe research and innovation program under the Marie Skłodowska-Curie grant agreement no. 101081280.

Author Contributions Milad Eskandarinia: Writing–original draft, conceptualization, investigation, methodology, validation, visualization, formal analysis, data curation, and resources. Elijah Adesanya: Writing–review and editing, data curation, investigation, validation, and supervision. Brant Walkley: Writing–review and editing, data curation, validation, and supervision. Juho Yliniemi: Writing–review and editing, project administration, data curation, validation, supervision, and funding acquisition.

Funding Open Access funding provided by University of Oulu (including Oulu University Hospital).

Data Availability Raw data of the analyses are available free of charge at https://doi.org/10.23729/fd-4f3d1e37-0d49-38d3-a86f-e9a53896df58.

Declarations

Conflict of interest The authors declare that they have no known competing financial interests or personal relationships that could have appeared to influence the work reported in this paper.

Open Access This article is licensed under a Creative Commons Attribution 4.0 International License, which permits use, sharing, adaptation, distribution and reproduction in any medium or format, as long as you give appropriate credit to the original author(s) and the source, provide a link to the Creative Commons licence, and indicate if changes were made. The images or other third party material in this article are included in the article's Creative Commons licence, unless indicated otherwise in a credit line to the material. If material is not included in the article's Creative Commons licence and your intended use is not permitted by statutory regulation or exceeds the permitted use, you will need to obtain permission directly from the copyright holder. To view a copy of this licence, visit http://creativecommons.org/licenses/by/4.0/.

References

1. US Geological Survey (2025) Mineral commodity summaries 2025. https://doi.org/10.3133/mcs2025
2. Fan C, Wei R, Cheng T et al (2024) The positive contributions of steel slag in reducing carbon dioxide emissions in the steel industry: waste heat recovery, carbon sequestration, and resource utilization. Chem Eng J 498:155379. https://doi.org/10.1016/J.CEJ.2024.155379
3. Das P, Upadhyay S, Dubey S, Singh KK (2021) Waste to wealth: recovery of value-added products from steel slag. J Environ Chem Eng 9:105640. https://doi.org/10.1016/J.JECE.2021.105640
4. Jiang Y, Ling TC, Shi C, Pan SY (2018) Characteristics of steel slags and their use in cement and concrete—a review. Resour Conserv Recycl 136:187–197. https://doi.org/10.1016/J.RESCONREC.2018.04.023
5. Brand AS, Fanijo EO (2020) A review of the influence of steel furnace slag type on the properties of cementitious composites. Appl Sci 10:8210. https://doi.org/10.3390/APP10228210

6. Martins ACP, de Franco Carvalho JM, Costa LCB et al (2021) Steel slags in cement-based composites: an ultimate review on characterization, applications and performance. Constr Build Mater 291:123265. https://doi.org/10.1016/J.CONBUILDMAT.2021.123265
7. Steindl FR, Doschek-Held K, Weisser K et al (2023) Mineral residues and by-products upcycled into reactive binder components for cementitious materials. RILEM Bookseries 44:153–164. https://doi.org/10.1007/978-3-031-33187-9_15
8. Benhelal E, Shamsaei E, Rashid MI (2021) Challenges against CO_2 abatement strategies in cement industry: a review. J Environ Sci 104:84–101. https://doi.org/10.1016/J.JES.2020.11.020
9. Li Y, Liu F, Yu F, Du T (2024) A review of the application of steel slag in concrete. Structures 63:106352. https://doi.org/10.1016/J.ISTRUC.2024.106352
10. Kriskova L, Pontikes Y, Cizer Ö et al (2012) Effect of mechanical activation on the hydraulic properties of stainless steel slags. Cem Concr Res 42:778–788. https://doi.org/10.1016/J.CEMCONRES.2012.02.016
11. Sajedi F (2012) Mechanical activation of cement–slag mortars. Constr Build Mater 26:41–48. https://doi.org/10.1016/J.CONBUILDMAT.2011.05.001
12. Wu F, Li H, Yang K (2021) Effects of mechanical activation on physical and chemical characteristics of coal-gasification slag. Coatings 11:902. https://doi.org/10.3390/COATINGS11080902
13. Singh SK, Jyoti VP (2021) Development of newer composite cement through mechano-chemical activation of steel slag. Constr Build Mater 268:121147. https://doi.org/10.1016/J.CONBUILDMAT.2020.121147
14. de Schutter A, Ceyssens L, Granata G, Van Gerven T (2024) Improving the carbonation of steel slags through concurrent wet milling. J Sustain Metall 10:1759–1773. https://doi.org/10.1007/s40831-024-00895-2
15. Wang H, Wu H, Tian J et al (2025) Resource utilization of lithium slag supplementary cementitious materials through mechanical activation: mechanism investigation and process optimization. Environ Res 283:122112. https://doi.org/10.1016/J.ENVRES.2025.122112
16. Zhao Y, Zheng Y, Cui K et al (2025) Development of ultrafine and highly reactive SCMs via combined CO_2 and mechanical activation of steel slag. Chem Eng J 516:163999. https://doi.org/10.1016/J.CEJ.2025.163999
17. Wang Q, Yang J, Yan P (2013) Cementitious properties of superfine steel slag. Powder Technol 245:35–39. https://doi.org/10.1016/J.POWTEC.2013.04.016
18. Li J, Ni W, Wang X et al (2022) Mechanical activation of medium basicity steel slag under dry condition for carbonation curing. J Build Eng 50:104123. https://doi.org/10.1016/J.JOBE.2022.104123
19. Sun X, Liu J, Zhao Y et al (2022) Mechanical activation of steel slag to prepare supplementary cementitious materials: a comparative research based on the particle size distribution, hydration, toxicity assessment and carbon dioxide emission. J Build Eng 60:105200. https://doi.org/10.1016/J.JOBE.2022.105200
20. Shen H, Forssberg E (2003) An overview of recovery of metals from slags. Waste Manag 23:933–949. https://doi.org/10.1016/S0956-053X(02)00164-2
21. Ghouleh Z, Guthrie RIL, Shao Y (2015) High-strength KOBM steel slag binder activated by carbonation. Constr Build Mater 99:175–183. https://doi.org/10.1016/J.CONBUILDMAT.2015.09.028
22. Pan SY, Adhikari R, Chen YH et al (2016) Integrated and innovative steel slag utilization for iron reclamation, green material production and CO_2 fixation via accelerated carbonation. J Clean Prod 137:617–631. https://doi.org/10.1016/J.JCLEPRO.2016.07.112
23. Kapeluszna E, Kotwica Ł (2022) The effect of various grinding aids on the properties of cement and its compatibility with acrylate-based superplasticizer. Materials 15:614. https://doi.org/10.3390/MA15020614
24. Li X, Mehdizadeh H, Ling TC (2023) Environmental, economic and engineering performances of aqueous carbonated steel slag powders as alternative material in cement pastes: influence of particle size. Sci Total Environ 903:166210. https://doi.org/10.1016/J.SCITOTENV.2023.166210
25. Xue K, Wan C, Xu Y et al (2022) Effect of pre-hydration age on phase assemblage, microstructure and compressive strength of CO_2 cured cement mortar. Constr Build Mater 325:126760. https://doi.org/10.1016/J.CONBUILDMAT.2022.126760
26. Zhang D, Cai X, Jaworska B (2020) Effect of pre-carbonation hydration on long-term hydration of carbonation-cured cement-based materials. Constr Build Mater 231:117122. https://doi.org/10.1016/J.CONBUILDMAT.2019.117122
27. Dubina E, Black L, Sieber R, Plank J (2010) Interaction of water vapour with anhydrous cement minerals. Adv Appl Ceram 109:260–268. https://doi.org/10.1179/174367509X12554402491029
28. Whittaker M, Dubina E, Al-Mutawa F et al (2013) The effect of prehydration on the engineering properties of CEM I Portland cement. Adv Cem Res 25:12–20. https://doi.org/10.1680/ADCR.12.00030
29. Chen T, Gao X (2019) Effect of carbonation curing regime on strength and microstructure of Portland cement paste. J CO2 Util 34:74–86. https://doi.org/10.1016/J.JCOU.2019.05.034
30. Lv L, Šavija B, Li L et al (2021) Prehydration of calcium sulfoaluminate (CSA) clinker at different relative humidities. Cem Concr Res 144:106423. https://doi.org/10.1016/J.CEMCONRES.2021.106423
31. Ramanathan S, Halee B, Suraneni P (2020) Effect of calcium sulfoaluminate cement prehydration on hydration and strength gain of calcium sulfoaluminate cement-ordinary portland cement mixtures. Cem Concr Compos 112:103694. https://doi.org/10.1016/J.CEMCONCOMP.2020.103694
32. Lv L, Luo S, Šavija B et al (2023) Effect of particle size distribution on the pre-hydration, hydration kinetics, and mechanical properties of calcium sulfoaluminate cement. Constr Build Mater 398:132497. https://doi.org/10.1016/J.CONBUILDMAT.2023.132497
33. Stoian J, Oey T, Bullard JW et al (2015) New insights into the prehydration of cement and its mitigation. Cem Concr Res 70:94–103. https://doi.org/10.1016/J.CEMCONRES.2015.01.012
34. Cieri L, Cassese P, Fabbrocino G et al (2023) Experimental study about the influence of storage conditions of bulk cement on the early-age stiffness evolution of cementitious pastes. Appl Sci 13:11734. https://doi.org/10.3390/APP132111734
35. ASTM C1897-20 Standard test methods for measuring the reactivity of supplementary cementitious materials by isothermal calorimetry and bound water measurements. https://www.astm.org/c1897-20.html. Accessed 15 Sep 2024
36. Eskandarinia M, Adesanya E, Walkley B, Yliniemi J (2025) Polycarboxylate ether as a grinding aid for basic oxygen furnace slag and its effects in blended cements. Submitted for peer-review in J Build Eng
37. Zhang Y, Zhang S, Chen Y, Çopuroğlu O (2022) The effect of slag chemistry on the reactivity of synthetic and commercial slags. Constr Build Mater 335:127493. https://doi.org/10.1016/J.CONBUILDMAT.2022.127493
38. Snellings R, Chwast J, Cizer Ö et al (2018) RILEM TC-238 SCM recommendation on hydration stoppage by solvent exchange for the study of hydrate assemblages. Mater Struct/

Materiaux et Constructions 51:1–4. https://doi.org/10.1617/s11527-018-1298-5
39. Lothenbach B, Durdziński P, De Weerdt K (2016) Thermogravimetric analysis, a practical guide to microstructural analysis of cementitious materials. CRC Press. https://doi.org/10.1201/B19074-5
40. Li X, Snellings R, Antoni M et al (2018) Reactivity tests for supplementary cementitious materials: RILEM TC 267-TRM phase 1. Mater Struct/Materiaux et Constructions 51:1–14. https://doi.org/10.1617/s11527-018-1269-x
41. EN 196-3 (2016) Methods of testing cement—part 3: determination of setting times and soundness. https://standards.iteh.ai/catalog/standards/sist/f27d98db-3199-4b2f-aa27-d891dc46be06/sist-en-196-3-2017
42. CEN/TC 444 Environmental characterization of solid matrices (2002) SFS-EN 12457–2, Characterisation of waste. Leaching. Compliance test for leaching of granular waste materials and sludges. Part 2: one stage batch test at a liquid to solid ratio of 10 l/kg for materials with particle size below 4 mm (without or with size reduction). https://sales.sfs.fi/en/index/tuotteet/SFS/CEN/ID2/1/4717.html.stx. Accessed 31 Aug 2025
43. Deng T, Garg V, Bradley MSA (2023) Electrostatic charging of fine powders and assessment of charge polarity using an inductive charge sensor. Nanomanufacturing 3(3):281–292. https://doi.org/10.3390/NANOMANUFACTURING3030018
44. Rescaglio A, Schockmel J, Vandewalle N, Lumay G (2017) Combined effect of moisture and electrostatic charges on powder flow. In: EPJ web of conferences. EDP sciences
45. Avet F, Snellings R, Alujas Diaz A et al (2016) Development of a new rapid, relevant and reliable (R3) test method to evaluate the pozzolanic reactivity of calcined kaolinitic clays. Cem Concr Res 85:1–11. https://doi.org/10.1016/J.CEMCONRES.2016.02.015
46. Jeon D, Jung S, Lee J, Moon J (2025) Investigating pozzolanic reactivity of ground ferronickel slag through the R3 test for its potential use as alternative supplementary cementitious material. Int J Concr Struct Mater 19(1):1–16. https://doi.org/10.1186/S40069-025-00832-X
47. Sivakumar PP, Matthys S, De Belie N, Gruyaert E (2021) Reactivity assessment of modified ferro silicate slag by R3 method. Appl Sci 11:366. https://doi.org/10.3390/APP11010366
48. Suraneni P, Hajibabaee A, Ramanathan S et al (2019) New insights from reactivity testing of supplementary cementitious materials. Cem Concr Compos 103:331–338. https://doi.org/10.1016/J.CEMCONCOMP.2019.05.017
49. Adediran A, Van Truong T, Perumal P (2025) Novel non-conventional raw materials as supplementary cementitious materials for low-carbon composite cement: chemical reactivity, fresh and hardened state characterization. Environ Res 271:121146. https://doi.org/10.1016/J.ENVRES.2025.121146
50. Williams SL, Beatty DN, Srubar W V. (2023) A small-scale thermogravimetric method to measure the chemical reactivity of supplementary cementitious materials. CEMENT 12:100071. https://doi.org/10.1016/J.CEMENT.2023.100071
51. Kalina RD, Al-Shmaisani S, Ferron RD, Juenger MCG (2019) False positives in ASTM C618 specifications for natural pozzolans. ACI Mater J 116:165–172. https://doi.org/10.14359/51712243
52. Scrivener K, Snellings R, Lothenbach B (2016) A practical guide to microstructural analysis of cementitious materials. 1–560. https://doi.org/10.1201/b19074
53. Kim T, Olek J (2012) Effects of sample preparation and interpretation of thermogravimetric curves on calcium hydroxide in hydrated pastes and mortars. Trans Res Record: J Trans Res Board. https://doi.org/10.3141/2290-02
54. de Azevedo BP, Estolano de Lima V, de Melo NA (2023) Capability of R3 test to evaluate pozzolanicity of ground raw and calcined sugarcane bagasse ashes. Mater Today Proc. https://doi.org/10.1016/J.MATPR.2023.04.048
55. Ramanathan S, Kasaniya M, Tuen M et al (2020) Linking reactivity test outputs to properties of cementitious pastes made with supplementary cementitious materials. Cem Concr Compos 114:103742. https://doi.org/10.1016/J.CEMCONCOMP.2020.103742
56. Frías M, Alujas A, Moreno-Reyes A et al (2024) Advances in understanding R3 chemical reactivity in various traditional and emerging pozzolans: chemical, mineralogical and calorimetric dimensions. Constr Build Mater 457:139474. https://doi.org/10.1016/J.CONBUILDMAT.2024.139474
57. Flegar M, Serdar M, Londono-Zuluaga D, Scrivener K (2020) Regional waste streams as potential raw materials for immediate implementation in cement production. Materials 13:5456. https://doi.org/10.3390/MA13235456
58. Vayghan AG, Horckmans L, Snellings R et al (2021) Use of treated non-ferrous metallurgical slags as supplementary cementitious materials in cementitious mixtures. Appl Sci 11:4028. https://doi.org/10.3390/APP11094028
59. Ju J, Zhang Q, Luo N et al (2024) Study on the hydration characteristics of steel slag cement. Constr Build Mater 420:135605. https://doi.org/10.1016/J.CONBUILDMAT.2024.135605
60. Han F, Zhang Z, Wang D, Yan P (2015) Hydration heat evolution and kinetics of blended cement containing steel slag at different temperatures. Thermochim Acta 605:43–51. https://doi.org/10.1016/J.TCA.2015.02.018
61. Zhang T, Ma B, Wu S et al (2022) Mechanical properties and hydration process of steel slag-cement binder containing nano-SiO2. Constr Build Mater 314:125660. https://doi.org/10.1016/J.CONBUILDMAT.2021.125660
62. Luo T, Wang X, Zhuang S (2023) Value-added utilization of steel slag as a hydration heat controlling material to prepare sustainable and green mass concrete. Case Stud Constr Mater 19:e02619. https://doi.org/10.1016/J.CSCM.2023.E02619
63. Briki Y, Zajac M, Haha MB, Scrivener K (2021) Factors affecting the reactivity of slag at early and late ages. Cem Concr Res 150:106604. https://doi.org/10.1016/J.CEMCONRES.2021.106604
64. Han F, Zhu Z, Zhang H et al (2024) Effect of steel slag on hydration kinetics and rheological properties of alkali-activated slag materials: a comparative study with fly ash. Materials 17:2260. https://doi.org/10.3390/MA17102260
65. John E, Lothenbach B (2023) Cement hydration mechanisms through time—a review. J Mater Sci 58:9805–9833. https://doi.org/10.1007/s10853-023-08651-9
66. Zhu L, Wang K, Wang Z et al (2023) Rheology of ultrafine tailings cemented paste backfill: the effect of the aqueous solution pH and superplasticiser dosage. Constr Build Mater 404:133270. https://doi.org/10.1016/J.CONBUILDMAT.2023.133270
67. Han F, Li Y, Jiao D (2023) Understanding the rheology and hydration behavior of cement paste with nickel slag. J Build Eng 73:106724. https://doi.org/10.1016/J.JOBE.2023.106724
68. Jiao D, Shi C, Yuan Q (2019) Time-dependent rheological behavior of cementitious paste under continuous shear mixing. Constr Build Mater 226:591–600. https://doi.org/10.1016/J.CONBUILDMAT.2019.07.316
69. Zhang Z, Jia Z, Shi J et al (2024) Understanding the dynamic rheological property of cement paste blended with steel slag powder: from interparticle force and physico-chemical parameters of view. Constr Build Mater 422:135826. https://doi.org/10.1016/J.CONBUILDMAT.2024.135826
70. Zhang D, Zhu T, Yang Q et al (2024) Influence of ground granulated blast furnace slag on recycled concrete powder-based

geopolymer cured at ambient temperature: rheology, mechanical properties, reaction kinetics and air-void characteristics. Constr Build Mater 438:137190. https://doi.org/10.1016/J.CONBUILDMAT.2024.137190
71. Chen Y, Zhang Y, Šavija B, Çopuroğlu O (2023) Fresh properties of limestone-calcined clay-slag cement pastes. Cem Concr Compos 138:104962. https://doi.org/10.1016/J.CEMCONCOMP.2023.104962
72. Deng XJ, Klein B, Zhang JX et al (2018) Time-dependent rheological behaviour of cemented backfill mixture. Int J Min Reclam Environ 32:145–162. https://doi.org/10.1080/17480930.2016.1239305
73. Pang L, Liao S, Wang D, An M (2022) Influence of steel slag fineness on the hydration of cement-steel slag composite pastes. J Build Eng 57:104866. https://doi.org/10.1016/J.JOBE.2022.104866
74. Hu S, He Y, Lu L, Ding Q (2006) Effect of fine steel slag powder on the early hydration process of portland cement. J Wuhan Univ Technol Mater Sci Ed 21:147–149. https://doi.org/10.1007/BF02861494/METRICS
75. Zhuang S, Wang Q (2021) Inhibition mechanisms of steel slag on the early-age hydration of cement. Cem Concr Res 140:106283. https://doi.org/10.1016/J.CEMCONRES.2020.106283
76. Zhu H, Ma M, He X et al (2021) Effect of wet-grinding steel slag on the properties of Portland cement: an activated method and rheology analysis. Constr Build Mater 286:122823. https://doi.org/10.1016/J.CONBUILDMAT.2021.122823
77. SFS (2012) SFS-EN 197–1, Suomen standardisoimisliitto, cement. Part 1: composition, specifications and conformity criteria for common cements. https://sales.sfs.fi/en/index/tuotteet/SFS/CEN/ID2/1/182891.html.stx. Accessed 7 Nov 2025
78. Pikasementti (CEM I 52.5)-Finnsementti. https://finnsementti.fi/tuotteet/sementit/pikasementti/. Accessed 7 Nov 2025
79. Zepper JCO, de Bruin S, Ling X et al (2024) Improving the early reactivity of activated basic oxygen furnace slag—the influence of particle fineness and grinding aids. J CO2 Util 83:102821. https://doi.org/10.1016/J.JCOU.2024.102821
80. Kim S, Yang J, Lee J et al (2025) Impact of triethanolamine on grinding and hydration performance of BOF steel slag blended cement. J Build Eng 101:111858. https://doi.org/10.1016/J.JOBE.2025.111858
81. Liu G, Tang Y, Wang J (2023) Effects of carbonation degree of semi-dry carbonated converter steel slag on the performance of blended cement mortar—reactivity, hydration, and strength. J Build Eng 63:105529. https://doi.org/10.1016/J.JOBE.2022.105529
82. Qiang W, Mengxiao S, Jun Y (2016) Influence of classified steel slag with particle sizes smaller than 20 μm on the properties of cement and concrete. Constr Build Mater 123:601–610. https://doi.org/10.1016/J.CONBUILDMAT.2016.07.042
83. Lothenbach B, Le Saout G, Gallucci E, Scrivener K (2008) Influence of limestone on the hydration of Portland cements. Cem Concr Res 38:848–860. https://doi.org/10.1016/J.CEMCONRES.2008.01.002
84. Zajac M, Rossberg A, Le Saout G, Lothenbach B (2014) Influence of limestone and anhydrite on the hydration of Portland cements. Cem Concr Compos 46:99–108. https://doi.org/10.1016/J.CEMCONCOMP.2013.11.007
85. Matschei T, Lothenbach B, Glasser FP (2007) The AFm phase in Portland cement. Cem Concr Res 37:118–130. https://doi.org/10.1016/J.CEMCONRES.2006.10.010
86. Kourounis S, Tsivilis S, Tsakiridis PE et al (2007) Properties and hydration of blended cements with steelmaking slag. Cem Concr Res 37:815–822. https://doi.org/10.1016/J.CEMCONRES.2007.03.008
87. Guo B, Liu B, Yang J, Zhang S (2017) The mechanisms of heavy metal immobilization by cementitious material treatments and thermal treatments: a review. J Environ Manage 193:410–422. https://doi.org/10.1016/J.JENVMAN.2017.02.026
88. Ahmed MJ, Schollbach K, van der Laan S, Brouwers HJH (2024) Reactivity of air granulated basic oxygen furnace steel slag and its immobilization of heavy metals. J Build Eng 91:109704. https://doi.org/10.1016/J.JOBE.2024.109704
89. European Union (2011) Regulation (EU) No 305/2011 of the European Parliament and of the Council of 9 March 2011 laying down harmonised conditions for the marketing of construction products and repealing council directive 89/106/EEC. Off J Europ Union. http://data.europa.eu/eli/reg/2011/305/oj
90. European Union (2002) Council Decision 2003/33/EC of 19 December 2002 establishing criteria and procedures for the acceptance of waste at landfills pursuant to article 16 of and annex II to directive 1999/31/EC. Official Journal of the European Union http://data.europa.eu/eli/dec/2003/33(1)/oj
91. Finnish Legislation (2017) Government decree on the recovery of certain wastes in Earth construction (MARA Decree 843/2017). Ministry of the Environment, Finland. https://www.finlex.fi/fi/lainsaadanto/saadoskokoelma/2017/843. Accessed 2 Sep 2025
92. Bundesministerium für Umwelt, Naturschutz, nukleare Sicherheit und Verbraucherschutz (BMUV) (2023) Ersatzbaustoffverordnung (EBV)—ordinance on substitute building materials (BGBl. I S. 212). Federal Republic of Germany. https://www.gesetze-im-internet.de/ersatzbaustoffv/BJNR259810021.html. Accessed 7 Nov 2025
93. Government of the Netherlands (2007, amended 2015) Soil quality decree (Besluit Bodemkwaliteit). Ministry of Infrastructure and Water Management, The Hagu. https://wetten.overheid.nl/BWBR0023085/2023-12-21. Accessed 7 Nov 2025
94. Piatak NM, Seal RR, Hoppe DA et al (2019) Geochemical characterization of iron and steel slag and its potential to remove phosphate and neutralize acid. Minerals 9(8):468. https://doi.org/10.3390/MIN9080468
95. Kapusta J, Dolníček Z, Sracek O, Malý K (2022) Origin of historical Ba-rich slags related to Pb–Ag production from Jihlava Ore district (Czech Republic). Minerals 12(8):985. https://doi.org/10.3390/MIN12080985
96. Lundstrom CC, Sutton AL, Chaussidon M et al (2006) Trace element partitioning between type B CAI melts and melilite and spinel: implications for trace element distribution during CAI formation. Geochim Cosmochim Acta 70:3421–3435. https://doi.org/10.1016/J.GCA.2006.04.014
97. Fällman AM (2000) Leaching of chromium and barium from steel slag in laboratory and field tests—a solubility controlled process? Waste Manag 20:149–154. https://doi.org/10.1016/S0956-053X(99)00313-X
98. Dayioglu AY (2024) Ph-dependent leaching characteristics of steel slag mitigated with water treatment residual. Geotech Test J 47:294–313. https://doi.org/10.1520/GTJ20220288
99. U.S. Environmental Protection Agency (EPA) (1992, amended 2021) Toxicity characteristic leaching procedure (TCLP), method 1311. In 40 CFR §261.24—toxicity characteristic. Code of federal regulations, Title 40: protection of environment. https://www.ecfr.gov/current/title-40/chapter-I/subchapter-I/part-261#p-261.24. Accessed 7 Nov 2025
100. Japanese Standards Association (JSA) (2013) JIS A 5011-1: slag aggregate for concrete—part 1: blast furnace slag aggregate. Japanese Industrial Standards Committee, Tokyo. https://webdesk.jsa.or.jp/books/W11M0090/index/?bunsyo_id=JIS+A+5011-1%3A2018. Accessed 7 Nov 2025
101. Japanese Standards Association (JSA) (2013) JIS A 6206: ground granulated blast-furnace slag for concrete. Japanese Industrial Standards Committee, Tokyo. https://webdesk.jsa.or.jp/

books/W11M0090/index/?bunsyo_id=JIS+A+6206%3A2024. Accessed 7 Nov 2025
102. Zhao Y, Qiu J, Ma Z, Sun X (2021) Eco-friendly treatment of coal gangue for its utilization as supplementary cementitious materials. J Clean Prod 285:124834. https://doi.org/10.1016/J.JCLEPRO.2020.124834

Publisher's Note Springer Nature remains neutral with regard to jurisdictional claims in published maps and institutional affiliations.